Spring 2023

Analysis of Dual-Element Antenna Configurations

Grant J. Evans

ANALYSIS OF DUAL-ELEMENT ANTENNA CONFIGURATIONS

by

GRANT J. EVANS

(Under the Direction of Professor Sungkyun Lim)

ABSTRACT

Dual-dipole antennas have been extensively researched previously for their bandwidth enhancing effect on Yagi type antennas. In this thesis, dual-dipole antennas are fabricated and measured. These experimental measurement results are verified with simulated values. First, a standard dual-dipole antenna is investigated and found that the high magnitude, opposite current directions on the dipole arms are the reasoning behind the creation of a high gain mode. This pattern is similar to a Yagi antenna. Next, a dual-band implementation of the dual-dipole antenna is shown, with two distinct resonances in a lower band and an upper band. Both bandwidths exhibit a dipole like mode, as well as a high gain mode. Finally, a dual-element cross-dipole antenna application is investigated. The antenna exhibits multiple dipole like modes within the bandwidth, high gain points, and CP generation at the center frequency.

INDEX WORDS: Bandwidth enhancement, Dipole antenna, Dual-band antenna, Double dipole, Dual-element dipole.

ANALYSIS OF DUAL-ELEMENT ANTENNA CONFIGURATIONS

by

GRANT J. EVANS

B.S., Georgia Southern University, 2021

M.S., Georgia Southern University, 2023

A Thesis Submitted to the Graduate Faculty of Georgia Southern University

in Partial Fulfillment of the Requirements for the Degree

MASTER OF SCIENCE IN ELECTRICAL ENGINEERING

STATESBORO, GEORGIA

ANALYSIS OF DUAL-ELEMENT ANTENNA CONFIGURATIONS

by

GRANT J. EVANS

Major Professor:	Sungkyun Lim
Committee:	Mohammad Ahad
	Fernando Rios-Gutierrez

Electronic Version Approved:

May 2023

DEDICATION

Firstly, I would like to thank my mom, Sylvia Evans, my dad, Geoffrey Evans, and my brother, Erik Evans. They make everything I do possible and support me in every way they can. I would also like to dedicate this to the Georgia Southern Fencing Team, it has provided me an outlet for the past 3 years that I wouldn't otherwise have had. Your support means everything to me.

ACKNOWLEDGMENTS

I would like to thank my advisor Dr. Sungkyun Lim for providing me with the opportunity to work in his laboratory and further my knowledge and passion in the field of antenna design. I would also like to thank my committee members Dr. Rios, and Dr. Ahad for taking the time to review my thesis. Additionally, I would like to thank my peers in the AWP lab for their advice and support throughout my time here. These peers include Kevin Leon, Mason Moore, John Verboom, Jack Nemec, and Jalexis Vanga Guzman.

TABLE OF CONTENTS

Page

LIST OF TABLES

Page

LIST OF FIGURES

Page

CHAPTER 1

INTRODUCTION

1.1 Dual-Dipole Antennas

The dual-element dipole is the connection of a standard λ/2 dipole to a secondary auxiliary dipole via the feeding line. The secondary auxiliary dipole length as well as spacing from the primary element can be changed depending on the application. Generally, the auxiliary dipole is very close in length to the original dipole, giving the antenna a slight bandwidth enhancement in comparison to a standard dipole. Dual dipoles can also be used to enhance the bandwidth of applications such as a Yagi-Uda antenna. Fig. 1.1 shows a single feed dual-dipole antenna.

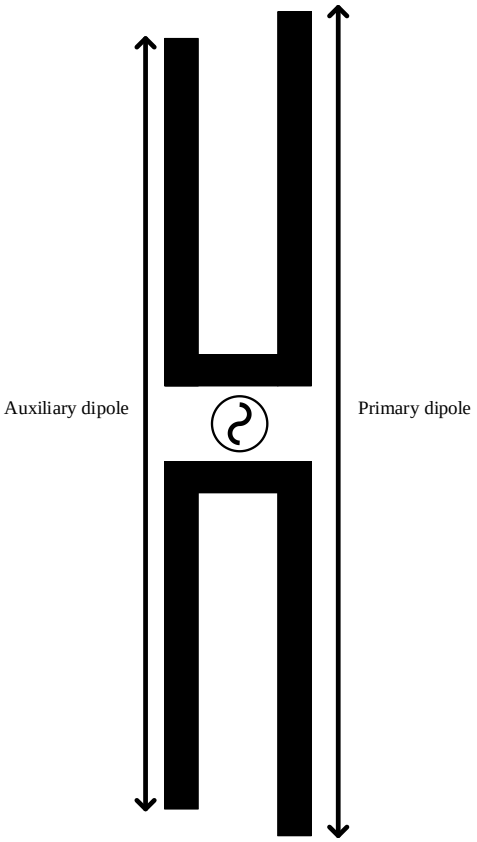

Fig. 1.1. Dual-dipole antenna

The dual-dipole antenna functions by combining the -10 dB impedance bandwidth (IBW) of the two dipole antennas. The -10dB IBW is a measure of how much power is reflected from the element. At -10 dB reflection coefficient the antenna is transmitting 90% of the power and reflecting 10% of it. This is considered a good match and is the standard for a transmitting or receiving antenna. When the two dipoles, primary and auxiliary are close in length, their reflection coefficients will combine to form a larger -10 dB impedance bandwidth, hence the bandwidth enhancing property of the dual-element dipole. A dual dipole is shown to bandwidth enhance a Yagi type antenna [1]. In this paper a dual-element dipole is used as shown in Fig. 1.2.

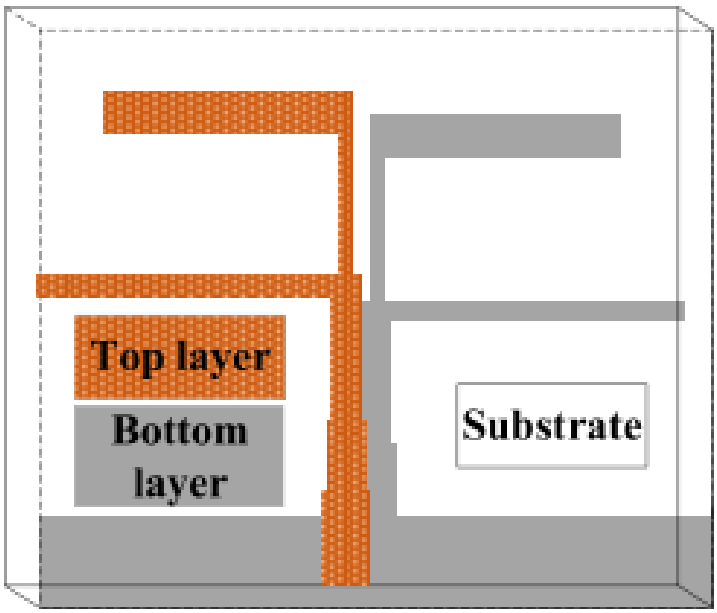

Fig. 1.2. Dual-element dipole [1].

In this configuration there are two dipoles connected to the feed, the larger element in the middle, and the smaller element on the top of the antenna. In this configuration the dual dipole is allowing for an increasement of the -10-dB impedance bandwidth, while also maintaining properties similar to that of a standard λ/2 dipole. Table I below shows a comparison of this antenna to other Yagi type antennas. The antenna in this configuration is “Dual-Element Dipole Yagi”. As seen when compared to other dual-band Yagi type antennas there is a noticeable bandwidth enhancement.

DUAL-BAND YAGI COMPARISON

Name	Center Freq. (GHz)	-10-dB IBW (%)	Minimum FBR (dB)
Dual-Band Yagi 1	9.5 & 10.3	5.9 & 2	19
Dual-Band Yagi 2	1.6 & 2.6	4 & 6.5	8
Dual-Element Dipole Yagi	4.38 & 6.85	19.4 & 14.6	9

Table I. Comparison of dual-element dipole to other Yagi type antennas [1].

The dual-element dipole is also shown to have other properties when the length difference is decreased, and spacing is increased over normal dual-dipole setups [2]. Three modes are shown in this paper, Dipole mode, with a standard dipole radiation pattern of 2 dBi realized gain. An omnidirectional radiation pattern in the azimuth plane is displayed, and nulls in the elevation plane when at the tips of the dipole. The next mode shown is at the combination point of the two dipoles, this is a high gain mode created at the point of dipole impedance bandwidth combination. This mode is known as "Yagi mode" and demonstrates a realized gain of 6.3 dBi. The next mode within the bandwidth is another "dipole mode", where a standard dipole pattern is again observed. This antenna also increases the standard dipole -10-dB impedance bandwidth from 10% to 16.7%. This configuration of the dual-element dipole is the main focus of this thesis.

1.2 Yagi-Uda Antennas

The Yagi-uda antenna is a type of high gain and directive antenna which is commonly used when those aspects are needed. The standard Yagi-uda is an antenna which is reliant on its parasitic elements to create high gain [3]. A standard 3-element Yagi consists of a driver, which is the fed element, as well as a reflector and director elements. These reflecting and directing elements are the parasitic elements in this form of antenna. Generally, the driver is a standard $\lambda/2$ dipole, while the reflecting element is about 1.05 times the driver length, and the directing element is about 0.95 times the driver length. These elements are

spaced anywhere from 0.15λ – 0.25λ away from each other. A standard 3-element Yagi is shown in Fig. 1.3.

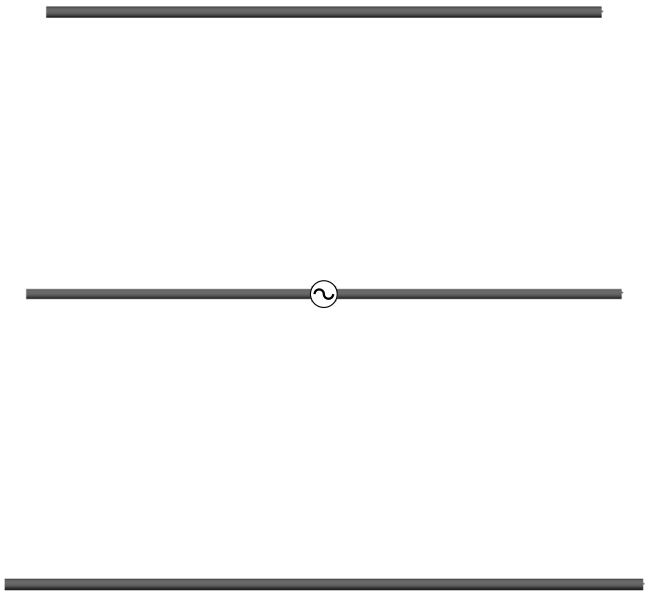

Fig. 1.3. Standard 3-element Yagi antenna.

The effect of adding parasitic elements up to 3 is shown in Table II [4]. In the table, 1 element is referring to just a standard halfwave dipole, where a standard 2 dBi realized gain can be seen. When extra elements are added a proportional gain increase is also observed. One drawback to this configuration of antenna however is the overall impedance bandwidth is decreased when parasitic elements are added. For example, in a full-size 3 element Yagi antenna the bandwidth is reduced by about 4% in comparison to a dipole.

Number of elements	Full-Sized / Size-Reduced	Area (cm^2)	-10-dB Impedance Bandwidth	Radiation Efficiency (η)	$B\eta$	Peak Realized Gain (dBi)
1	Full-Sized	-	9.9%	99.3%	0.099	2.0
	Size-Reduced	15.4	8.2%	99.1%	0.081	1.8
2	Full-Sized	55.6	8.0%	99.4%	0.080	3.9
	Size-Reduced	45.5	6.6%	99.5%	0.066	3.4
3	Full-Sized	87.1	6.5%	99.7%	0.065	8.3
	Size-Reduced	63.1	6.1%	99.8%	0.061	7.6

Table II. Gain increasement of Yagi antennas. [4]

The high gain of the Yagi antenna is a product of the swapping currents on each element. This current direction swapping is shown in Fig. 1.4. This effect is what generates the high gain point of a Yagi type antenna.

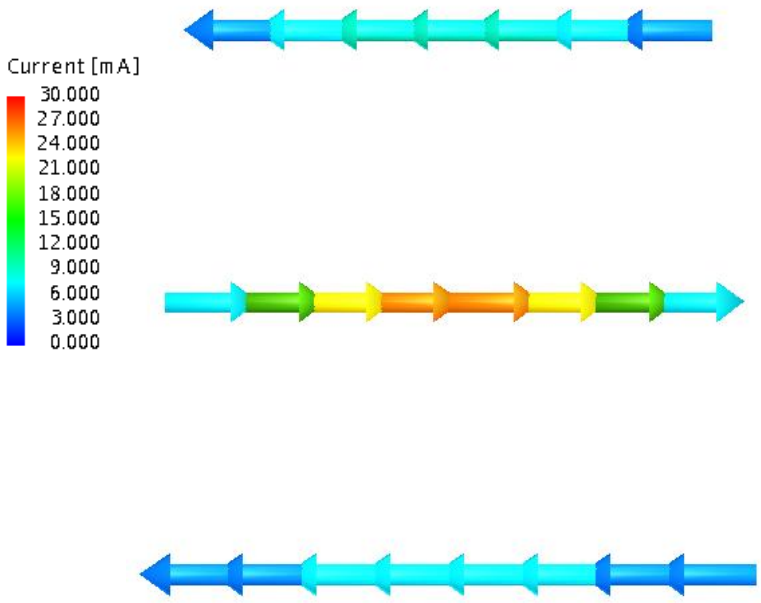

Fig. 1.4. Currents in a standard 3-element Yagi.

1.3 Dual-band Antennas

When an antenna operates in two distinct frequency bands it is referred to as dual band. If applications require multiple frequency bands to function it is more practical to use a single antenna than two separate antennas to fulfill the same function. This single antenna in multiple frequency bands reduces the amount of overall space needed for the application. Some examples of applications requiring multiple frequency bands is Wi-Fi. Wi-Fi uses the frequency bands of 2.4 GHz and 5 GHz. If a single antenna is able to cover both bandwidths, the amount of space that the router takes up can be physically reduced. A prototype dual-band antenna with a ground plane is shown in [5]. This antenna accomplishes a dual-band resonance at 2.4 GHz and 5.8 GHz. It does this through changing the lengths of the strips L_1 and L_2. The antenna is shown in Fig. 1.5.

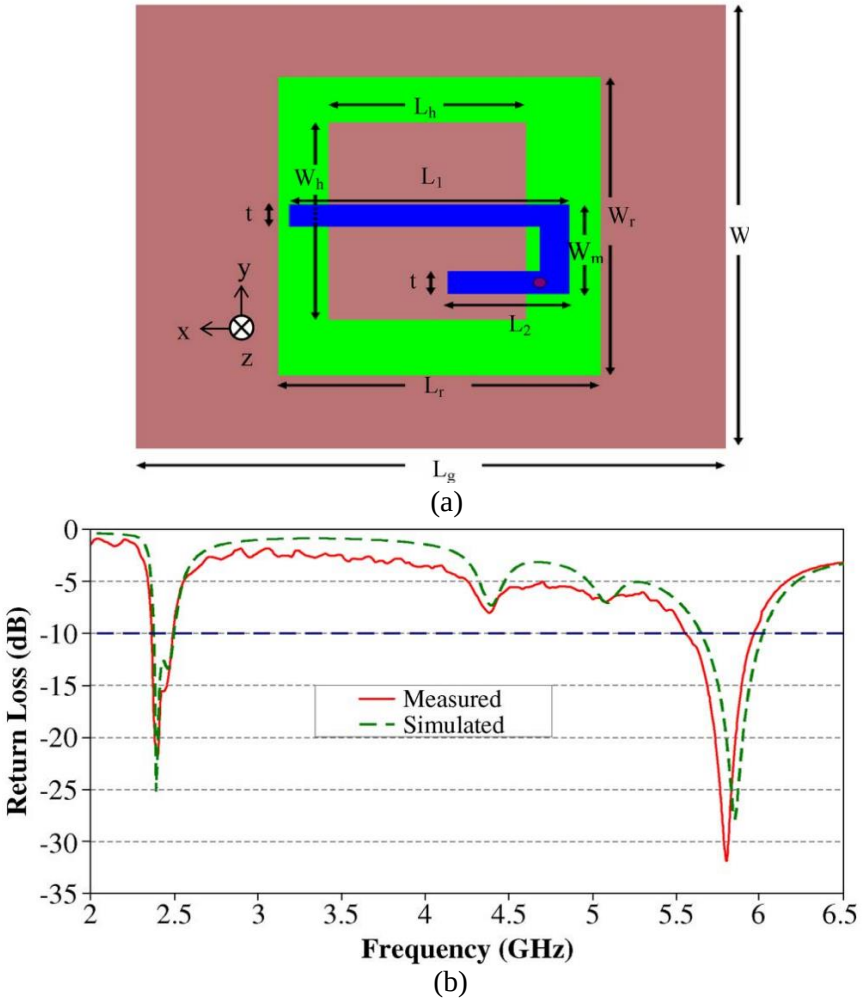

Fig. 1.5. (a) Prototype dual-band antenna, and (b) Reflection coefficient versus frequency [5].

Each length L_1 and L_2 affect the resonance location of the lower band and upper band respectfully. As seen the different lengths cause a strong current to be located on the arm of L_1 in the lower band, and L_2 in the upper band.

1.4 Circular Polarization

Circular polarization (CP) is a type of polarization in which the electric field rotates during propagation, negating the need for a polarization match. In CP antennas there are however two different types of polarization, left-handed (LH), and right-handed (RH) CP. This just denotes which way the field is rotating, with a left-handedness or a right-handedness. CP and elliptical polarization (EP) is measured

using axial ratio (AR), the equation for AR is shown in Equation 2 [6]. In this equation P_{dB} is the cross-polar power which is defined by Equation 1.

$$P_{dB} = |P_{RHCP} - P_{LHCP}|$$

Equation 1. Cross-polar power

$$AR = 20log_{10}\left(\frac{1 + 10^{\left(\frac{-P_{dB}}{20}\right)}}{1 - 10^{\left(\frac{-P_{dB}}{20}\right)}}\right)$$

Equation 2. Axial ratio

Any AR value above 3 dB denotes that the antenna is Elliptically polarized (EP). An AR of 3 dB or less denotes that the antenna is CP. When the antenna is at 0 dB AR it is perfectly CP. As the axial ratio is a function of the cross polar power, the difference between P_{RHCP} and P_{LHCP} is what determines the AR value and if it is circularly polarized or not. One common way to create CP is covered in this thesis, the cross-dipole. A standard cross-dipole antenna is shown in Fig. 1.6.

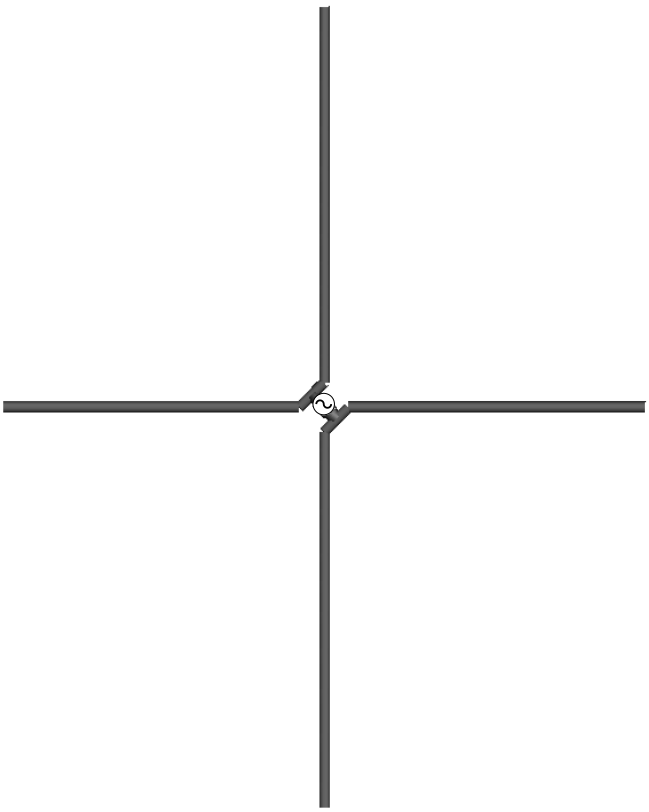

Fig. 1.6. Standard cross-dipole antenna.

The antenna is composed of a λ/2 dipole, and a secondary dipole of approximately 85% of the length of the λ/2 dipole connected perpendicularly. This length difference in the cross-dipole antenna generates an equal magnitude current, with a phase difference of 90°. This equal magnitude and 90° phase difference in the currents generates CP. A spacing reduced cross-dipole is shown in Fig. 1.7(a) [7]. This antenna works on the same operating principle as a standard cross-dipole, the only difference is the top loading and the introduction of a parasitic directing element. As shown in Fig. 1.7(b), the axial ratio dips below 3 dB, and creates an axial ratio bandwidth (ARBW) of 1%.

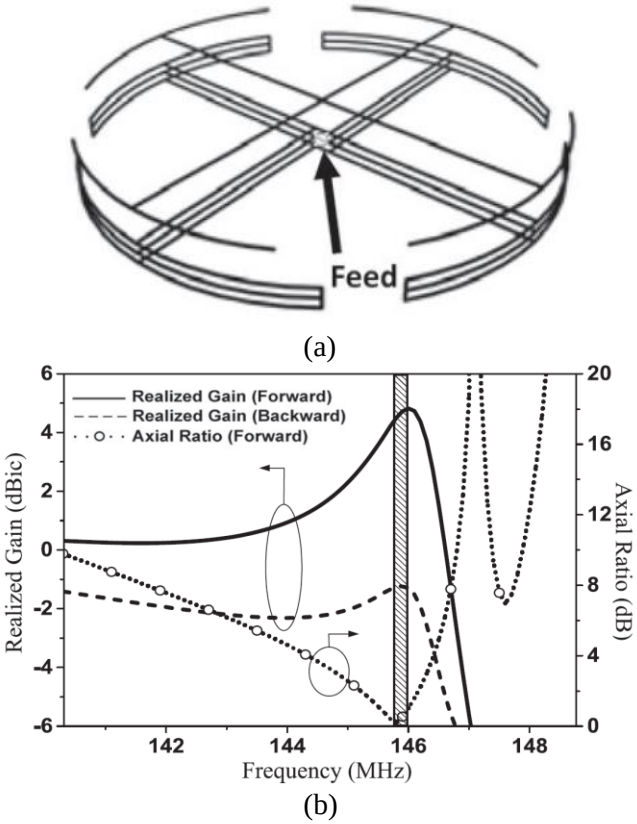

Fig. 1.7. (a) Spacing reduced cross-dipole antenna, and (b) axial ratio and realized gain [7].

1.5 Antenna Measurement

After simulation of an antenna is complete and results have been obtained, fabrication must be performed to ensure that it matches the simulated values given. All fabricated antenna measurements in this thesis are performed in an Anechoic chamber which is rated between 1 and 40 GHz. Pyramid shaped foam

absorbers on walls of the chamber minimize reflection from within the chamber. Aluminum sheets line the walls underneath the foam absorbers forming a complete seal of the chamber from outside interference. The anechoic chamber used in these measurements is shown in Fig. 1.8.

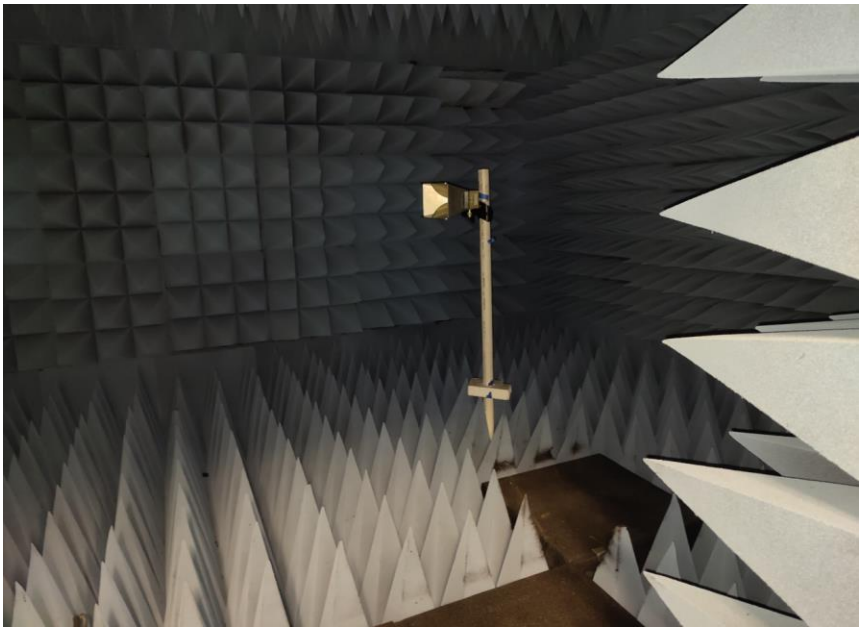

Fig. 1.8. Anechoic chamber

Fig. 1.9. Agilent E5063A

Two TDK horn antennas operating between 1 and 18 GHz are used a control, as their gain values are known and constant. An Agilent E5063A vector network analyzer is used to capture the S_{11} (reflection) and S_{21} (transmission) values. The vector network analyzer used is shown in Fig. 1.9. For comparison from

measurement to simulation values the S_{11} and S_{21} values must be taken from the network analyzer and used to calculate antenna parameters such as realized gain, and AR. Equation 3 shows the realized gain calculation from the S_{21}, and known gain parameters of the two TDK horn antennas. Where RG is the realized gain, G_H is the known gain value of the horn antenna, and $H_{S_{21}}$ is the S_{21} of the standard TDK horn antenna to the measuring TDK horn antenna.

$$RG = G_H - \left(|S_{21}| - \left|H_{S_{21}}\right|\right)$$

Equation 3. Realized gain calculation in measurement.

Next, steps must be taken to ensure that the measurement values received are not subject to error. Simulation values are performed in a free space, lossless environment. Measurement setup must mimic this scenario to ensure a good match between simulated and measured values of the antennas. In this thesis a Krytar model 4010265 180° hybrid balun is used to balance the power being fed to the antenna. The Hybrid balun used in these measurements is shown in Fig. 1.10.

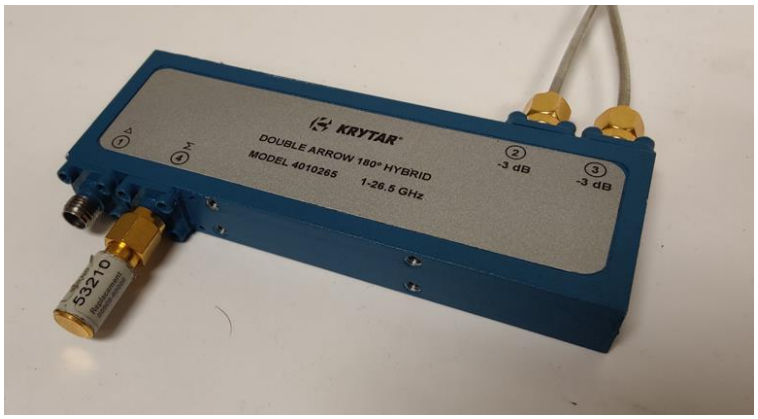

Fig. 1.10. Krytar model 4010265 180° hybrid balun

1.6 Thesis Objective

Dual-element dipoles have been used extensively in the past for bandwidth enhancement of Yagi-type antennas, as well as length reduction in LPDA's. However, when the dual dipole is introduced with a larger length difference between the primary and auxiliary dipole, as well as a small spacing ($.09\lambda$) a point of high gain is created. The goal of this thesis is so analyzing different applications of dual-dipole antennas on their own, instead of their integration into a larger array. A standard dual dipole is investigated first,

where the feeding element is moved to the middle, and the front-to-back ratio present in previous designs is nearly eliminated. The dual dipole is then investigated for the reasoning behind the creation of high gain at the combination point of the two dipoles. Next, the dual dipole concept is applied in a dual-band antenna application. Two dual-dipole antennas are created at separate resonant frequencies, then combined at the feed to create a dual-band antenna, with both a dipole like mode, as well as a high gain mode in both bandwidths. Finally, the last topic also takes two dual dipoles with separate resonant frequencies and combines them at the feed. This time however the design is similar to a cross-dipole antenna. Dipole mode is again observed, and two points of high gain are created as well as CP generation in the middle dipole mode.

CHAPTER 2

ANALYSIS OF A DUAL-ELEMENT DIPOLE

2.1 Abstract

A single feed dual-element dipole is analyzed in this chapter. The dual-element dipole with a spacing of 0.09λ is shown to generate a point of high gain in the +z direction. The reasoning behind this is shown to be the cause of close spacing between the two dipoles. The proposed antenna is simulated and measured for validation of the values obtained. The measured -10-dB IBW is 20.9% (1.395 GHz – 1.721 GHz). The peak realized gain in the +z direction is shown to be 6.36 dBi at 1.568 GHz. The measured front-to-back ratio at this point is 17.2 dB.

2.2 Introduction

Dipoles are commonly used antennas in modern communication systems by nature its omni-directional radiation pattern in the azimuth plane and approximately 2 dBi of gain across their bandwidth. They are a reliable antenna to build more complex designs off due to their simplistic and predictable nature. Extensive research has previously been published on improving the dipole design. Antenna's such as a Yagi-Uda are designed to improve the gain of the dipole array [8-16]. This is performed by adding parasitic elements spaced from around 0.15λ - 0.25λ away from other elements. One drawback of this design is the reduced impedance bandwidth (IBW). A size reduced, spacing reduced, 3-element Yagi with folding is investigated [8]. A -10-dB IBW of 1.9% is observed. Some improvements can be made to this reduced impedance bandwidth as found in [4], where a 15-element size-reduced Yagi is investigated. While the realized gain is 13.3 dBi, however, the -10-dB IBW is less than 5%, making the antenna very narrow band.

These Yagi antennas can be further improved with the use of a double dipole, or dual-dipole antenna. Dual-dipole antennas have been shown to enhance the bandwidth of Yagi-Uda antennas. A planar dual-dipole antenna is shown to enhance the bandwidth of a 3-element Yagi antenna to 78.4% -10-dB IBW [17] while maintaining a stable gain of 6.4-7.4 dBi. The bandwidth enhancing properties of the dual-element

dipole can also be applied to Log-periodic Dipole antennas [18]. Where in comparison to other LPDA's of similar build, the bandwidth is slightly enhanced and the overall length of the antenna is reduced by 0.1λ. Dual-dipole antennas have also been used in broadband applications [19,20]. In these broadband applications the dual-dipole resonances are combined at a point where the -10-dB impedance bandwidth is maximized. These antennas also function well on their own with just a single feed [20], [2]. A dual-dipole spacing analysis is performed in [2] and is found to display high gain characteristics (6.3 dBi) at the combination point of the two dipoles.

In this chapter, the dual-dipole antenna is redesigned and investigated. By redesigning the feed location, the front-to-back ratio is lowered out of the high gain mode. In Section II, the design procedure is explained and an investigation is performed into why the point of high gain is created between two connected dipoles. All simulations are performed in Altair FEKO 2021. In Section III a prototype is built and measured for verification. The wire radius of the design is fixed at 0.5 mm (AWG 18). The antenna is measured in an anechoic chamber using an Agilent Technologies E5063A network analyzer.

2.3 Antenna Design Procedure

A standard $\lambda/2$ dipole is investigated in Fig. 2.1(a). A second, larger dipole is constructed to where the edge of the two dipoles -10-dB IBW points intersect, this is shown in Fig. 2, with dipole 1 and dipole 2. The two dipoles used are shown in Fig. 2.1(b), constructed with two separately excited feeds matched at a characteristic 50-Ω impedance. The reflection coefficient is shown assuming the dipoles are completely isolated from each other. The two dipoles are then connected together in Fig. 2.1(c). The feed is placed on the larger dipole as noted in [2]. The resulting reflection coefficient is shown in Fig. 2.2, the total combined -10-dB IBW is 16.7% (1.444 GHz – 1.707 GHz). The peak realized gain is noted as 6.3 dBi in the $+z$ direction, shown in Fig. 2.3. There is a point of high realized gain in the $-z$ direction after the combination point. To solve this issue the feeding point is moved to the middle of the two dipoles, shown in Fig. 2.1(d).

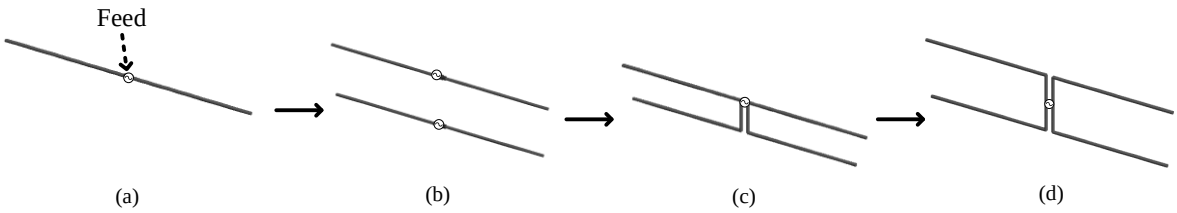

Fig 2.1. Design procedure of a dual-element dipole; (a) Standard dipole, (b) two dipoles with separately excited feeds, (c) Single feed dual-element dipole with feed on top, and (d) dual-element dipole with feed in the middle.

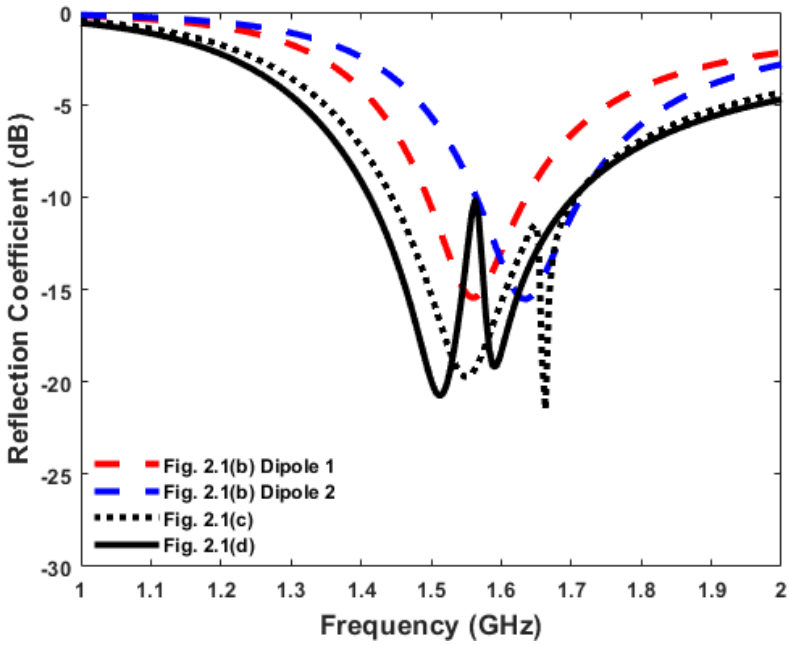

Fig 2.2. Dual-element dipole with two single dipoles comparison reflection coefficient versus frequency.

The spacing between the two dipoles is also increased to .09λ to allow for bandwidth combination. The resulting reflection coefficient is 19.3% -10-dB IBW (1.406 GHz – 1.707 GHz), shown in Fig. 2.2. The peak realized gain decreased slightly (0.2 dBi difference), however the front-to-back ratio after the combination point was removed. This is shown in Fig. 2.3.

The geometry of the proposed antenna is shown in Fig. 2.4. The side view is shown with dimensions, and an isometric view is also shown for reference. The feed is placed in the middle as outlined in the study above, and to achieve the point of high realized gain in the +z direction the larger dipole is placed above the smaller dipole in the +z direction [2]. This dual-dipole configuration is investigated for the reasoning behind why there is a small peak point of realized gain at the combination point of the two dipoles.

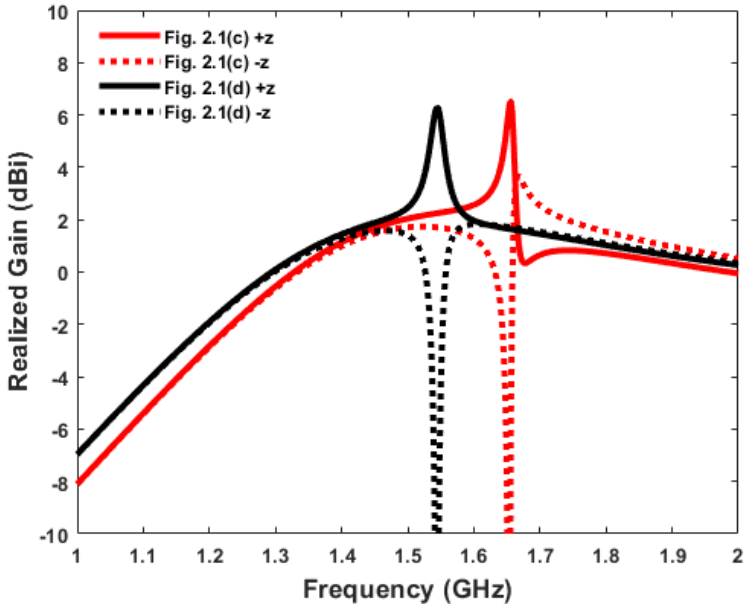

Fig 2.3. Realized gain comparison between Fig. 2.1(c) and Fig. 2.1(d).

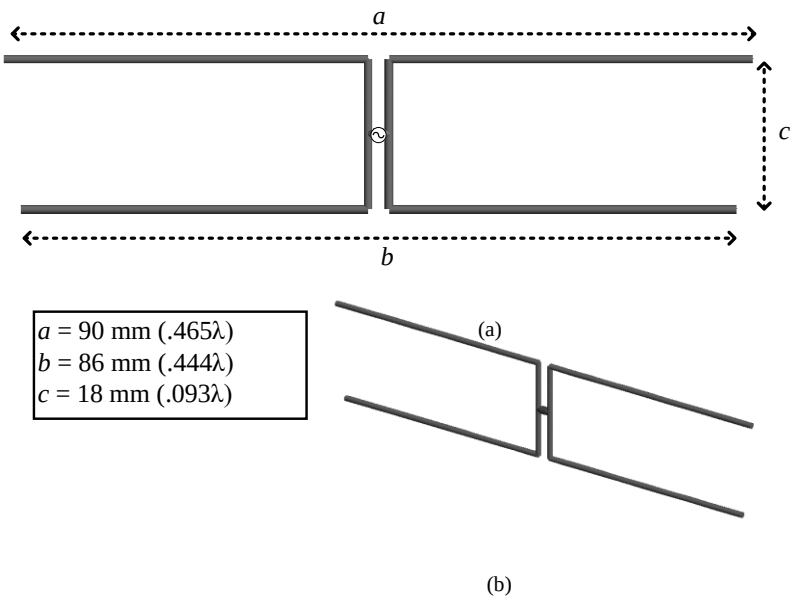

Fig 2.4. Dual-Element dipole configuration: (a) side view; (b) slanted view.

The dual-element dipole is noticed to operate at an anti-resonance in the impedance versus frequency plot, shown in Fig. 2.5(b). A standard dipole impedance versus frequency is shown in Fig. 2.5(a) for reference. This provides a solid understanding as to why the combination point peak gain displays a small bandwidth.

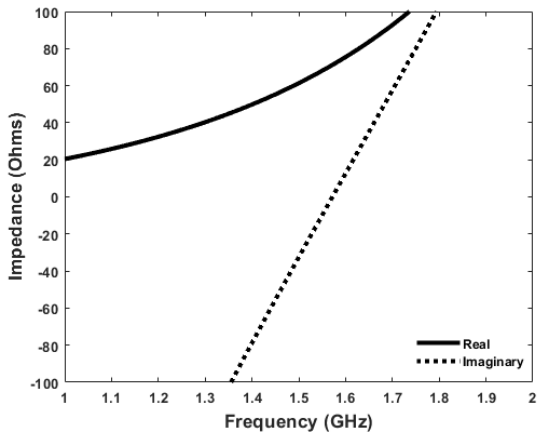

(a)

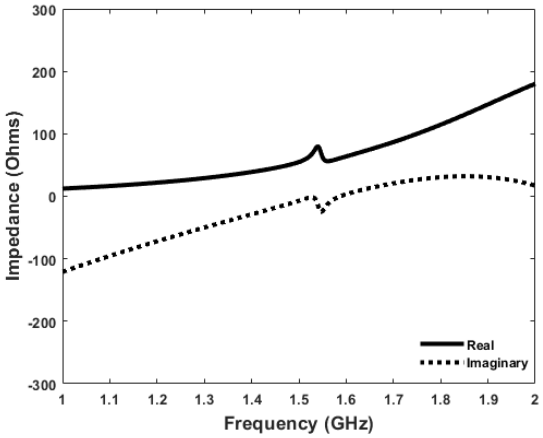

(b)

Fig. 2.5. (a) Standard half-wavelength dipole impedance versus frequency, and (b) dual-dipole impedance versus frequency.

Next an investigation is performed between the dual-element dipole in Fig. 2.3, and two independently fed dipoles. All variables from the design are kept similar, a = 90 mm (.465λ), b = 86 mm (.444λ), and c = 18 mm (.093λ). The only difference between the designs is the removal of the connecting elements between the dipoles. A comparison of the gain versus frequency in the +z and -z direction is performed in Fig. 2.6(a). A design reference is also provided in the figure, showing which curve belongs to each design. As shown the gain plots are similar, the single feed design displays a peak gain of 6.57 dBi at 1.543 GHz, while the two feed design displays a peak gain of 6.3 dBi at 1.62 GHz. The frequency shift between the designs is because of the added electrical length from the connecting elements at the feed in the single feed design. This study is consistent with [21], which states that the closer spacing of an array of isotropic radiators

increases the directivity. However, normally as spacing decreases between radiators, matching would also decrease. The single feed design prevents this by connecting the independent radiators to the same feed. The circuit equivalent of the dual-element dipole is shown in Fig. 2.6(b). A parallel connection of the two elements ensures the exciting voltage is balanced between the two connected dipoles.

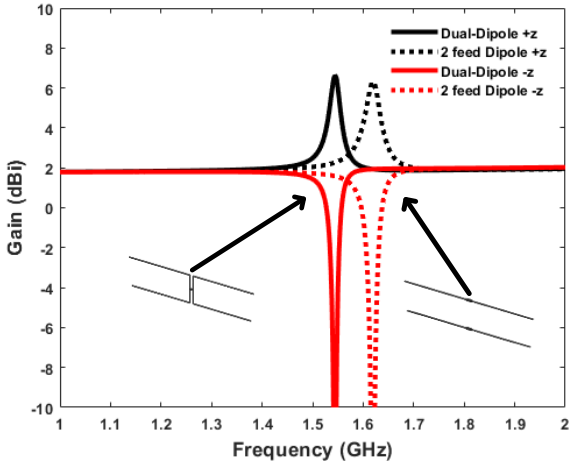

(a)

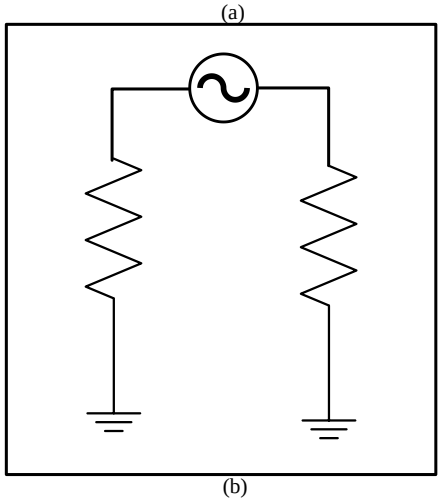

(b)

Fig. 2.6. (a) Gain comparison between dual-dipole and two independently fed dipoles, and (b) circuit diagram of dual-element dipole antenna.

Next, currents in the dual-element dipole are analyzed to confirm which elements are active at certain points in the frequency range. The points 1.46 GHz, 1.54 GHz, and 1.58 GHz were selected as these correspond to a “dipole mode”, a high gain mode, and another “dipole mode” in the upper bandwidth. The currents were analyzed at each phase, the only the peak magnitude phase is shown. The first current shown is the first “dipole mode” at 1.46GHz in Fig. 2.7(a).

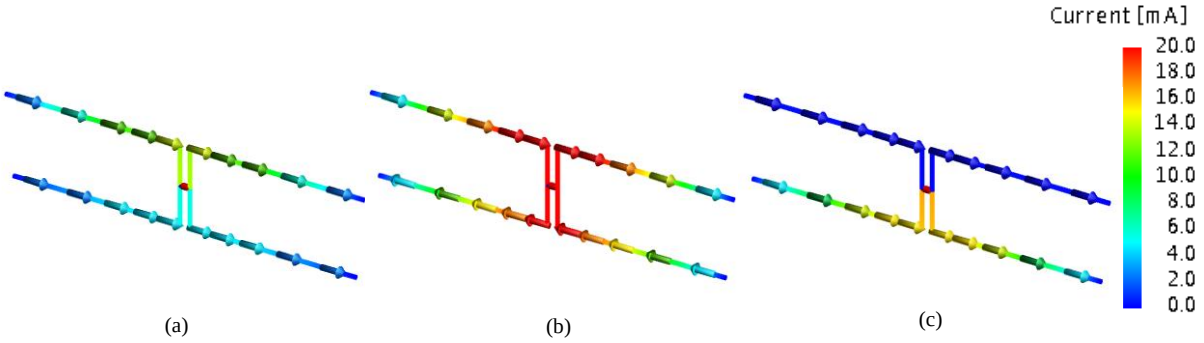

Fig. 2.7. Currents at (a) 1.46 GHz 0° phase, (b) 1.54 GHz 90° phase, and (c) 1.58 GHz 10° phase.

Both currents in the dipole arms are moving toward the +*y* direction, and as expected the top dipole has the highest magnitude of current. A small current is seen in the bottom dipole, however, there is a slight front-to-back ratio at this point (.04 dB), so a small amount of current is expected. Next, the currents at the combination point are shown in Fig. 2.7(b). As this is the point of peak gain for the antenna both elements are active, the currents are shown at 90° phase as this is the peak current magnitude for both elements. Both elements are active, and the currents are moving in opposite directions. The antenna is functioning in this mode similar to a Yagi antenna, where the currents in each element compared to the past element are in opposite direction. Finally, the last "dipole mode" is shown at 1.58 GHz in Fig. 2.7(c). In this mode there is 0 front-to-back ratio, and this is verified in the currents as there is negligible current flowing in the bottom dipole. Similar to the first "dipole mode" the currents in both dipoles are flowing in the same direction.

Fig. 2.8. Prototype of the proposed antenna.

2.4 Measurement Verification

A prototype of the single feed dual-element dipole antenna is fabricated for validation of the findings in simulation. The fabricated antenna is shown in Fig. 2.8. Measurement is performed using an Agilent Technologies E5063A network analyzer. The feeding mechanism of the antenna is made up of standard SMA coaxial cables that are connected to the two -3-dB ports of a Krytar model 4010265 180-degree hybrid balun (frequency band: 1 GHz - 26.5 GHz). All measurements are performed in an anechoic chamber rated for use from 1 GHz – 40 GHz.

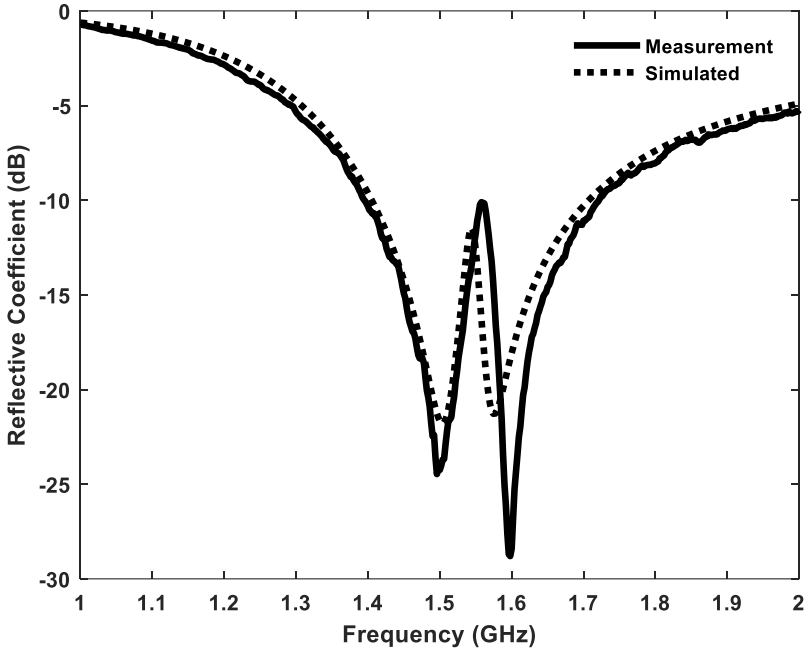

Fig. 2.9. Simulated and measured reflection coefficient versus frequency.

Fig. 2.9 displays the simulated and measured reflection coefficient versus frequency. The measured -10-dB IBW of the fabricated antenna is 20.9% (1.395 GHz – 1.721 GHz). Due to minor errors during fabrication the combination point is shifted up in frequency minimally. The overall bandwidth shows a good agreement between simulation and measurement.

The simulated and measured realized gain versus frequency in the +*z* and -*z* direction is shown in Fig. 2.10. The measured peak realized gain is 6.36 dBi at 1.568 GHz. The front-to-back ratio at this point is 17.2

dB. As stated previously, the combination point is slightly shifted up in frequency, therefore the point of realized gain is also shifted upwards. The trend of the measured realized gain is similar, showing a good agreement to simulation. The slight front-to-back ratio in the measured results likely a product of the solder used during fabrication.

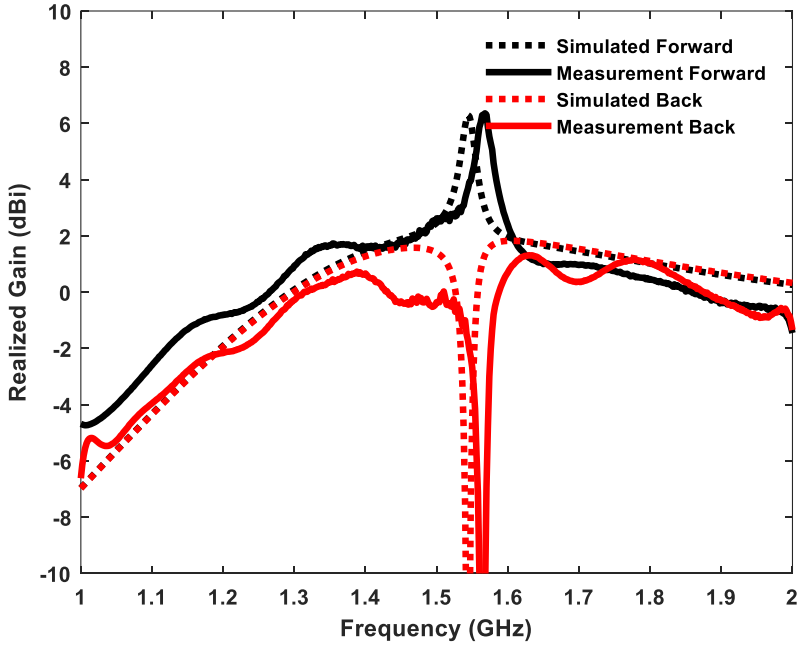

Fig. 2.10. Simulated and measured realized gain versus frequency.

Finally, in Fig. 7 the normalized radiation patterns versus angle are shown. Fig. 2.11(a)(d), displays the XZ and YZ patterns respectively at 1.46 GHz. This frequency point is the first instance of "dipole mode", with an omnidirectional radiation pattern in the azimuth plane, and two nulls at the tips of the dipole in the elevation plane. The measured the radiation patterns provide a good match to simulation. The next point at 1.54 GHz is shown in Fig. 2.11(b)(d). This is the point of high realized gain at the combination point, as expected there is a high directivity toward to +*z* direction, and a high front-to-back ratio in the -*z* direction. The final point at 1.58 GHz is in Fig. 2.11(c)(f). This is another "dipole mode", as expected the patterns follow a similar trend to Fig. 2.11(a)(d) with an omnidirectional pattern in the azimuth plane, and two nulls in the elevation plane. Overall, the measurements show a good agreement to simulation.

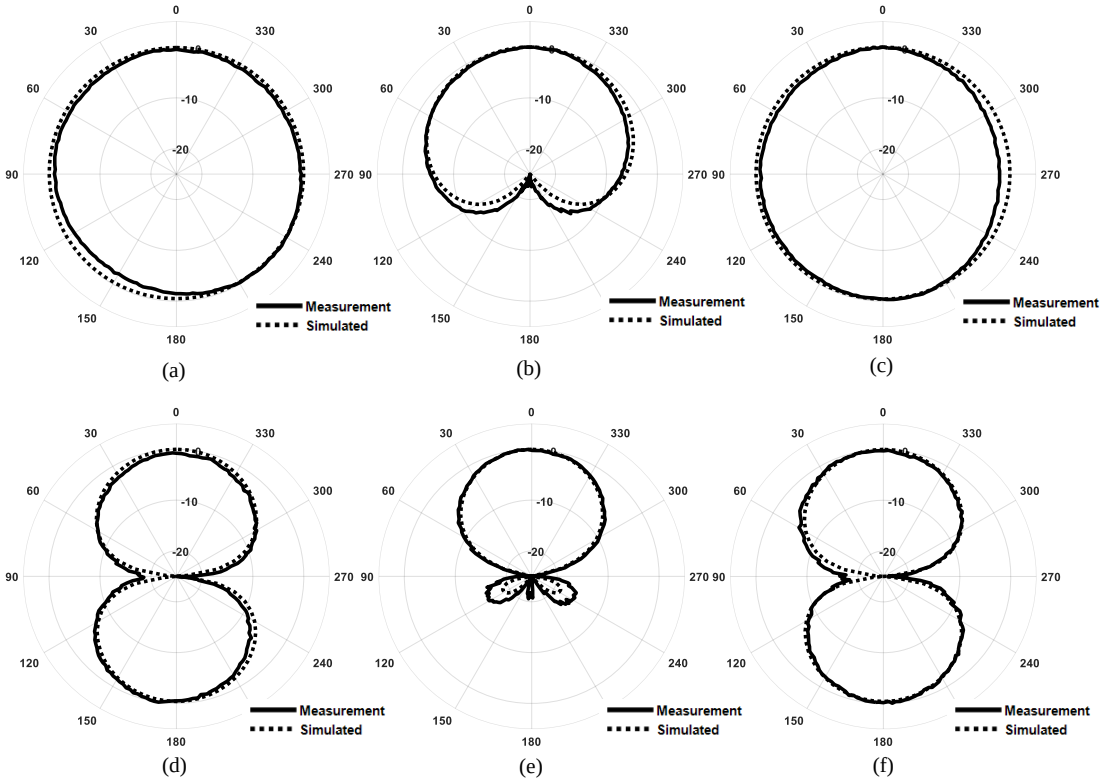

Fig. 2.11. Simulated and measured normalized radiation patterns of the proposed antenna; at the frequency of (a) 1.46 XZ, (b) 1.54 XZ, (c) 1.58 XZ, (d) 1.46 YZ, (e) 1.54 YZ, and (d) 1.58 YZ.

2.5 Conclusion

A dual-dipole antenna is created with (0.09λ) spacing between the two dipole elements and a point of high gain is shown at the combination point. Firstly, a study is performed on the design of a dual-dipole antenna, two dipoles are created at frequencies where their -10-dB IBW intersects. Connecting elements are then added, and a feed location is determined to be best in the middle of the two dipoles. The created dual-dipole is then investigated, and it is determined that the small bandwidth of the point of high gain is due to the antiresonance created when the dipoles are conjoined. Two modes are observed, with the larger dipole active in the lower bandwidth causing a “dipole mode” to be created. At the combination point both elements are observed to be active where the point of high gain is created, with mostly equal and opposite direction currents. In the upper bandwidth the smaller dipole is solely active, creating another “dipole

mode". The agreement between simulation and measurement is good. The antenna displays a -10-dB IBW of 20.9% (1.395 GHz – 1.721 GHz). The peak realized gain is observed to be 6.36 dBi at 1.568 GHz, and the normalized XZ and YZ radiation patterns match well with simulated values.

CHAPTER 3

DESIGN OF A DUAL-BAND, QUAD-ELEMENT DIPOLE ANTENNA

3.1 Abstract

A quad-element dipole with dual-band capabilities is displayed in this chapter. The antenna is composed of two orthogonal dual-element dipoles with separate resonant frequencies. The lower band element is oriented in the +*z* direction, while the upper band element is oriented in the +*x* direction. The simulated antenna is fabricated and measured for validation of the obtained simulation values. A -10-dB IBW of 19.0% (1.368 GHz – 1.655 GHZ) in the lower band, and 10.2% (1.960 GHz – 2.170 GHz) is observed in the upper band. A peak realized gain in the +*z* direction is noted at 6.3 dBi, with a front-to-back ratio of 19.8 dB. A peak realized gain point is also noted in the lower band, with a value of 6.2 dBi, and a front-to-back ratio of 26.6 dB.

3.2 Introduction

Dual-band antennas are becoming increasingly popular due to the ability of a single antenna to replace what would originally be two antennas. A dual-band antenna is defined as an antenna that operates in two separate frequency bands. Dual-band antennas have been extensively researched in [22-36]. A dual-band antenna is shown to achieve a broad bandwidth with use of a double-sided patch antenna [22]. Another antenna with multiple resonators attached to a single feed is shown to achieve a dual-band resonance [23-25]. An omni-directional antenna is shown to achieve dual-band capabilities [26]. These omni-directional antennas in this dual-band mode are extremely useful for applications such as Wi-fi.

Omni-directional patterns in the azimuth plane can be achieved by dipole. A magno-electric dipole combination is used to achieve dual-band capabilities in [27-29]. This setup is similar to the dual-dipole. A dual-dipole application of dual-band antennas are shown in [30-33], where two standard dipoles are used and connected together at the feed. This generates a dual-band resonance. Although having an omnidirectional pattern is good for some applications, other applications require high gain antennas. Dual-

band, dual-dipole antennas are used to generate high gain by implementing parasitic elements to increase the total gain [34-36]. High gain can also be achieved at the combination point of the dual-element dipole without parasitic elements [2].

In this chapter, a quad-element dipole is introduced. First, two separate dual-element dipoles are created at different frequency bands. These elements are analyzed individually and then combined together at the feed. By combining these two separate antennas together two distinct resonances are formed. A point of high gain is created in each bandwidth, as well as an omnidirectional radiation pattern in the azimuth plane. FEKO is used for all simulations. A prototype antenna is fabricated and measured for verification. The wire radius of the design is 0.5 mm (AWG 18). The dual-band antenna is measured using an Agilent Technologies E5063A network analyzer. All measurements on the fabricated antenna are performed in an anechoic chamber.

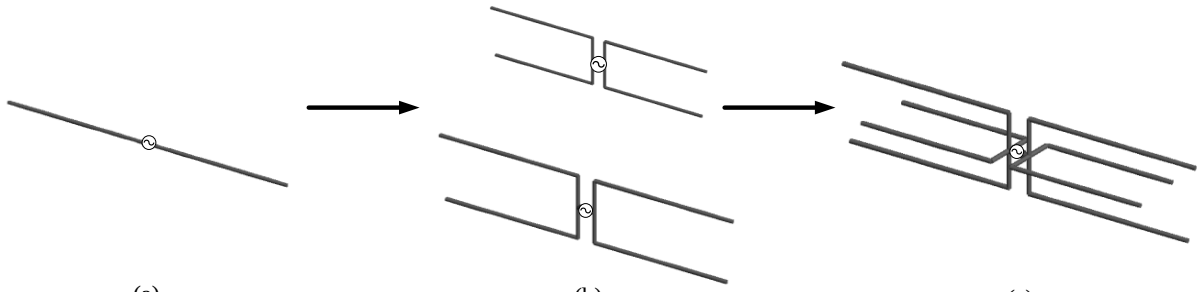

Fig. 3.1. Detailed design procedure of a quad-element dipole. (a) Standard halfwave dipole, (b) two dual element dipoles, and (c) proposed antenna.

3.3 Antenna Design Procedure

The design procedure for this antenna design is shown in Fig. 3.1. In Fig. 3.1(a) a standard $\lambda/2$ dipole is created, standard results are observed from it, 10% -10-dB impedance bandwidth (IBW), 2 dBi realized gain across the frequency range. Next a second dipole is created to where the -10-dB IBW of the second dipole lines up under -10-dB with the first dipole. This creates the dual-element dipole. Two of which are then created at separate frequency bands, λ_1 = 1.52 GHz and denotes the center frequency of the first created dual-element dipole. The next, smaller dual-element dipole is created at λ_2 = 2.02 GHz. These created dual-

element dipoles are shown in Fig. 3.1(b). The resulting reflection coefficient of the two independently is shown in Fig. 3.2.

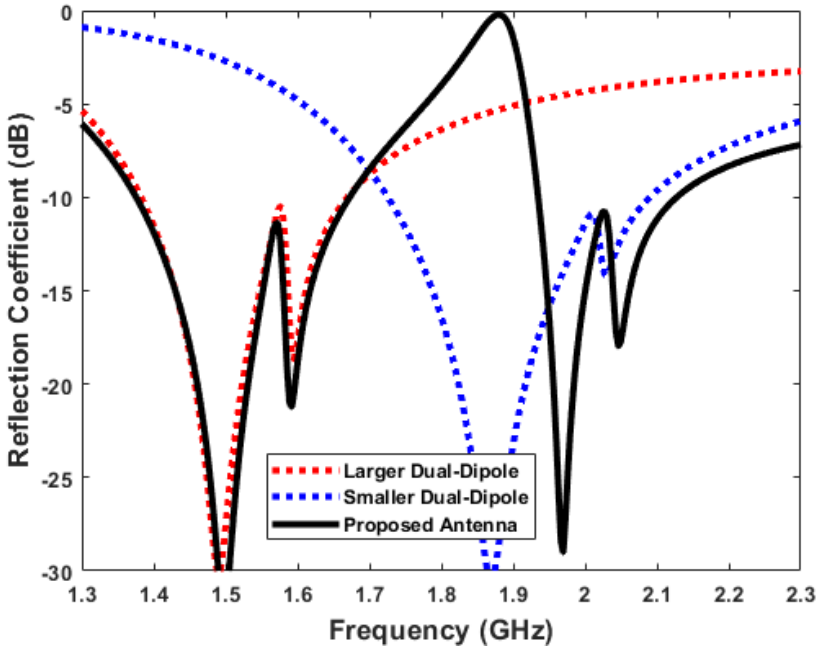

Fig 3.2. Reflection coefficient versus frequency of Fig. 3.1(b)(c).

Next, the two separate dual-element dipoles are combined at the feed, with the smaller dual-dipole antenna rotated by $\theta = 90°$ toward the $+x$ direction. This antenna configuration is shown in Fig. 3.1(c). The resulting reflection coefficient versus frequency is shown in Fig. 3.2. A comparison between the quad-element dipole and the elements it is composed of is shown. While the lower band remains mostly the same bandwidth wise, the upper band loses -10-dB IBW when combined with the larger element. The simulated -10-dB IBW values for the lower band is 19.4% (1.377-1.673 GHz), and the upper band is 9.6% (1.930-2.124 GHz). With each of their combination points being located at 1.576 GHz and 2.02 GHz for the lower and upper band respectfully. Dual-element dipoles are shown to propagate toward the larger element when close spacing is introduced [2]. The realized gain versus frequency comparison of the quad-element dipole

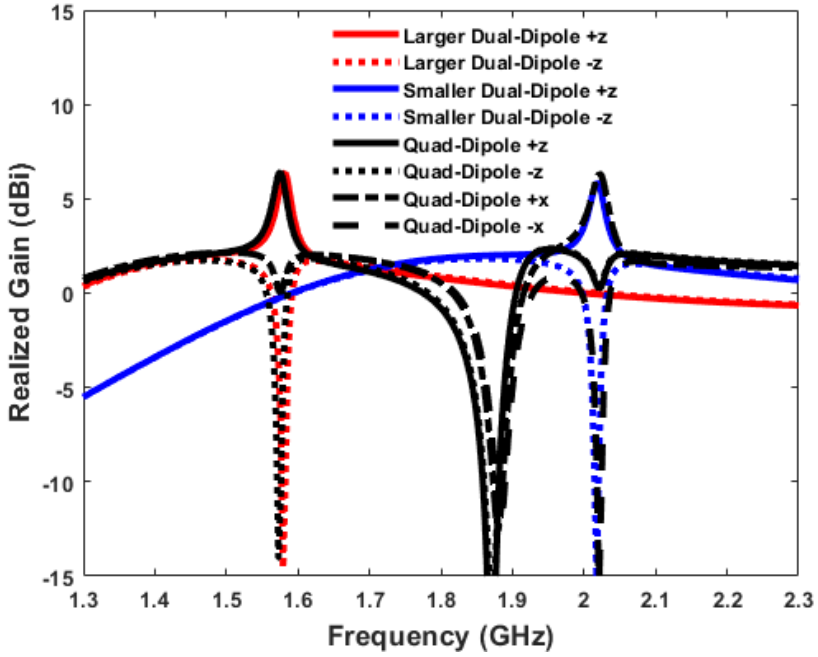

Fig 3.3. Realized gain versus frequency of Fig. 3.1(b)(c).

to its composing elements is shown in Fig. 3.3. The realized gain of both the composing elements, and the quad-element dipole is 6.4 dBi in the lower band at 1.58 GHz, and 6.3 dBi in the upper band at 2.02 GHz. The realized gain upper band is shown in the +*x* and -*x* direction, and the lower band is shown in the +*z* and -*z* direction. In both bands three distinct modes of operation are shown, for example, in the lower band at 1.48 GHz a "dipole mode" is shown, with no front-to-back ratio, and an omnidirectional radiation pattern in the azimuth plane. Next at 1.58 GHz a high gain point is created at the combination point of the dual-element dipole in the lower band. This point has a high front-to-back ratio (20.1 dB). Next, at 1.62 GHz another "dipole mode" is displayed, with minimal front-to-back ratio and an omnidirectional radiation pattern in the azimuth plane. The same characteristics are mimicked in the upper band, just shifted in frequency.

Next, the impedance versus frequency plots of the quad-element dipole and its composing elements are shown in Fig. 3.4. In Fig. 3.4(a) the two composing elements of the quad-element dipole are shown.

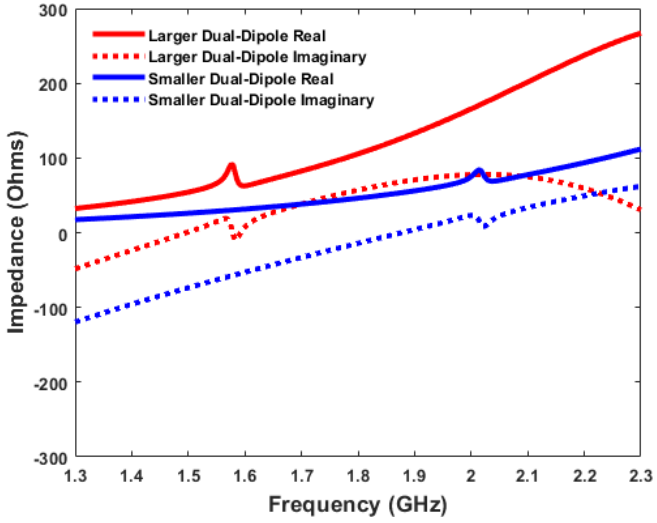

(a)

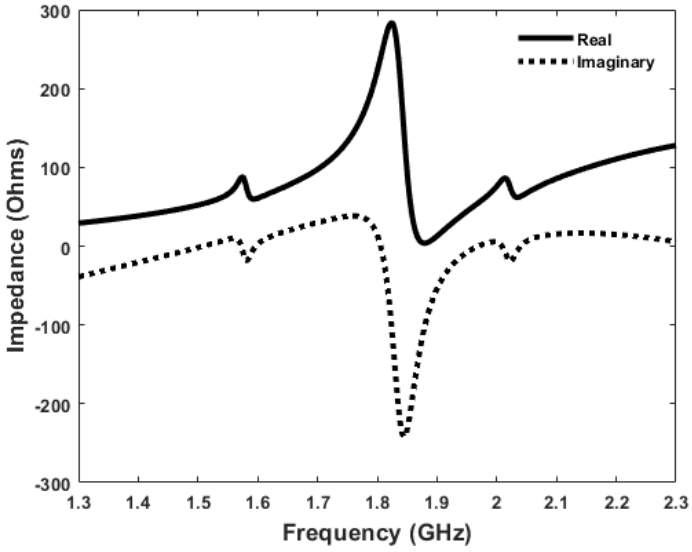

(b)

Fig. 3.4. Impedance versus frequency of (a) Fig. 3.1(b), and (b) Fig. 3.1(c).

The combination point is operating at an anti-resonance, which explains the small bandwidth of the high gain point. The impedance plots at this point are similar, just shifted in frequency as expected with the reduction in size of the smaller dual-element dipole. Fig. 3.4(b) displays the impedance versus frequency of the combined quad-element dipole. The combination points at the antiresonances are still present at the same locations as the original two elements. The only difference is the spike in Rin, and the drop in Xin at

the point where the reflection coefficient is equal to 0 dB. Other than the spike, the trend of the combined quad-element dipole follows the same trend as the two dual-element dipoles that make it up.

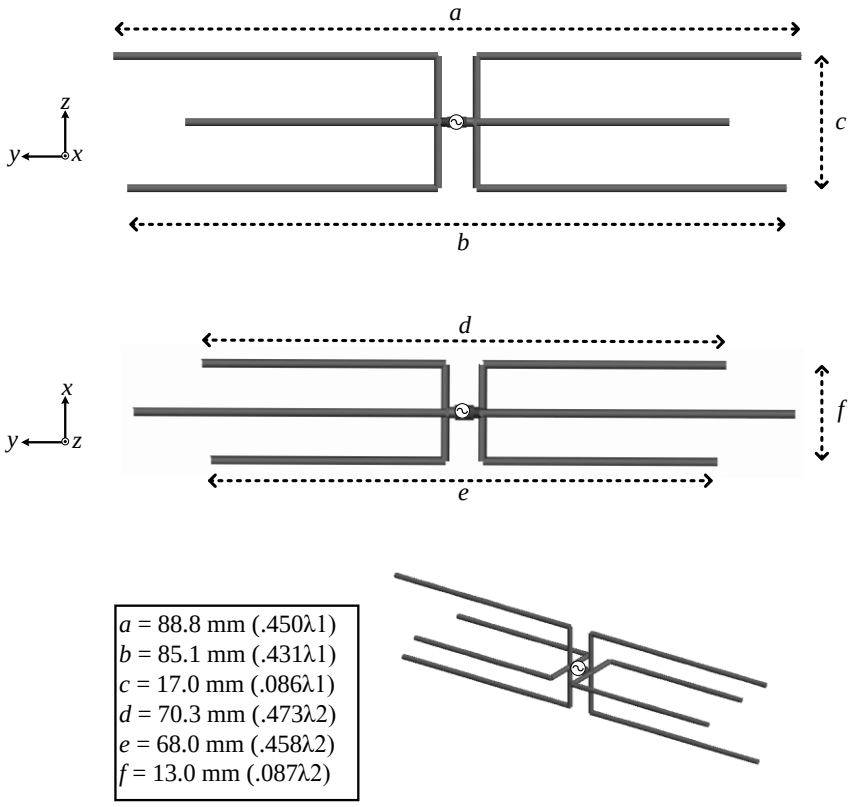

Fig. 3.5. Detailed geometry of the proposed antenna.

Next, the geometry of the proposed quad-element dipole is shown in Fig. 3.5. The spacing between the the dual-element dipoles is $0.086\lambda_1$ in the lower band oriented in the $+z$ direction, and $0.087\lambda_2$ in the upper band oriented in the $+x$ direction. The lengths of the dual-element dipole in the lower band, oriented in the $+z$ direction are $0.450\lambda_1$ for the longer dipole, and $0.431\lambda_1$ for the smaller dipole. In the upper band, oriented in the $+x$ direction the longer dipole element is at a length of $0.473\lambda_2$. The shorter dipole length is $0.458\lambda_2$. With this orientation the point of realized gain in the lower band is propagating toward the $+z$ direction, and $+x$ in the upper band. Finally, the currents in each band are shown in Fig. 3.6. The frequency to display the current at is chosen at each of the following modes of operation. The current chosen is the phase with the highest magnitude of current in both dipole arms that would be resonating.

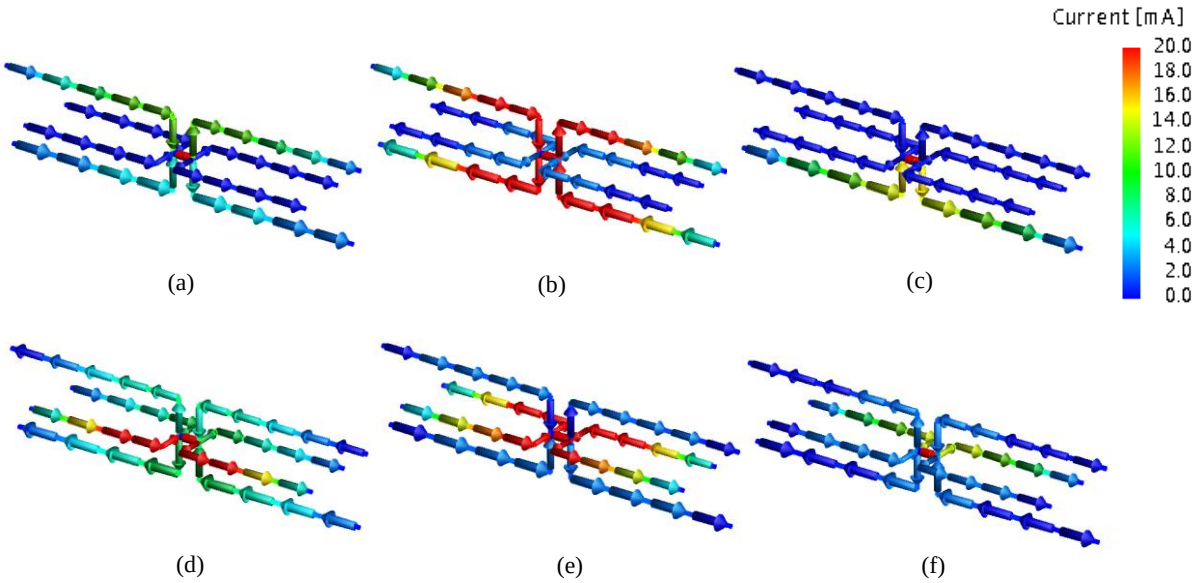

Fig. 3.6. Current analysis of a quad-element dipole. (a) 1.480 GHz 10° phase, (b) 1.580 GHz 130° phase, (c) 1.620 GHz 30° phase, (d) 1.956 GHz 0° phase, (e) 2.024 GHz 110° phase, and (f) 2.075 GHz 30° phase.

The first current shown is in Fig. 3.6(a), this is the first "dipole mode" pattern, the main element active is the larger dipole in the zenith direction. There is a small current magnitude in the smaller dipole, and there is a corresponding slight front-to-back ratio (0.26 dB). This current contributes to this front-to-back ratio, but it is minimal, and the main resonating element is the large dipole. Next, shown in Fig. 3.6(b) is the peak realized gain point in the lower band, both elements are active, hence the combination point. The currents are moving in opposite directions, much like a Yagi-Uda antenna. This equal and opposite current direction contributes to the high realized gain point. Next the currents at the last "dipole mode" of the lower band are shown in Fig. 3.6(c). The only element active is the smaller dipole located in the -*z* direction. The "dipole mode" is present due to the single dipole being the only active element. The currents in the upper band are shown next, the first "dipole mode" current is shown in Fig. 3.6(d). Due to the small frequency difference between the two bands (1.58 GHz, 2.02 GHz) there are minimal currents in the two lower band elements, as well as the smaller upper band element. There is again a front-to-back ratio at this point (1.42 dB). The high realized gain point in the +x direction, within the upper band is shown next in Fig. 3.6(e). Similar to the lower band high realized gain point, the two elements are both active, and show strong and opposite current directions. The last point shown is Fig. 3.6(f), at this point the only element active is the smaller

dipole in the upper band. This element being the only one active behaves similarly to Fig. 3.6(c) in the lower band, due to only the dipole being active, a dipole like radiation pattern is observed at this point.

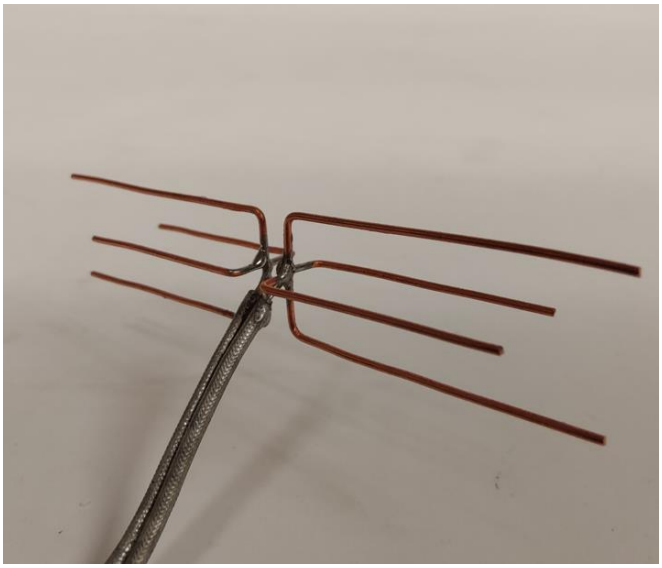

Fig. 3.7. Proposed Antenna.

3.4 Measurement Verification

A prototype of the quad-element dipole antenna is fabricated for verification of the results found in simulation. The fabricated antenna is shown in Fig. 3.7. The antenna is measured using an Agilent Technologies E5063A vector network analyzer. A Krytar model 4010265 180-degree hybrid balun (1 – 26.5 GHz) is used to connect the antenna to the vector network analyzer. Two coaxial SMA cables are connected to the output ports, and a 50-Ω load is applied to the sum port to ensure equal power distribution to the antenna. The simulated and measured reflection coefficient versus frequency is shown in Fig. 3.8. The measured -10-dB IBW for the lower band is 19.0% (1.268 GHz – 1.655 GHz), the upper band is 10.2% (1.960 GHz – 2.170 GHz). The lower band displays an excellent match to simulation, in the upper band a slight frequency shift is noticed, however the combination point is noted to be the same. This minor frequency shift in the upper band is likely due to the solder used in the fabrication process.

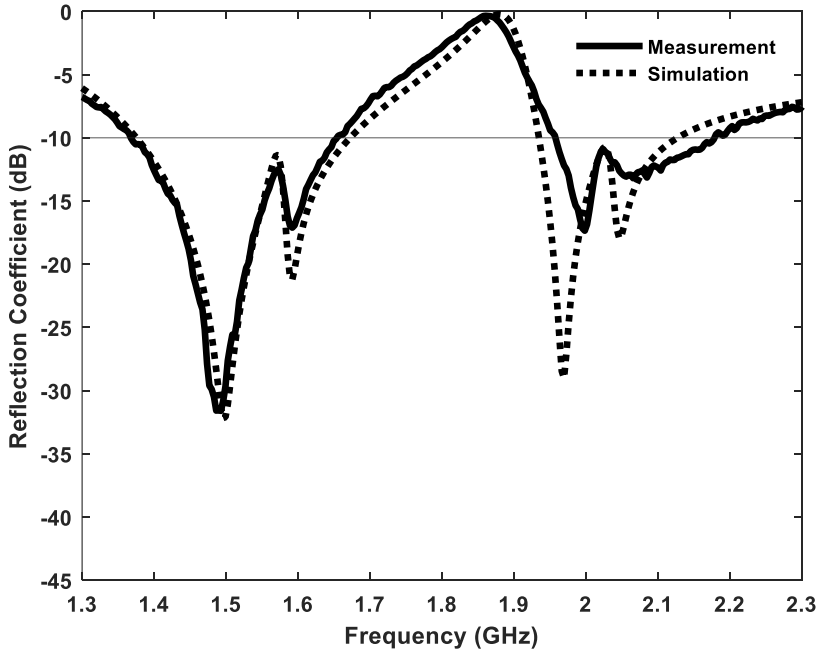

Fig. 3.8. Simulated and measured reflection coefficient versus frequency.

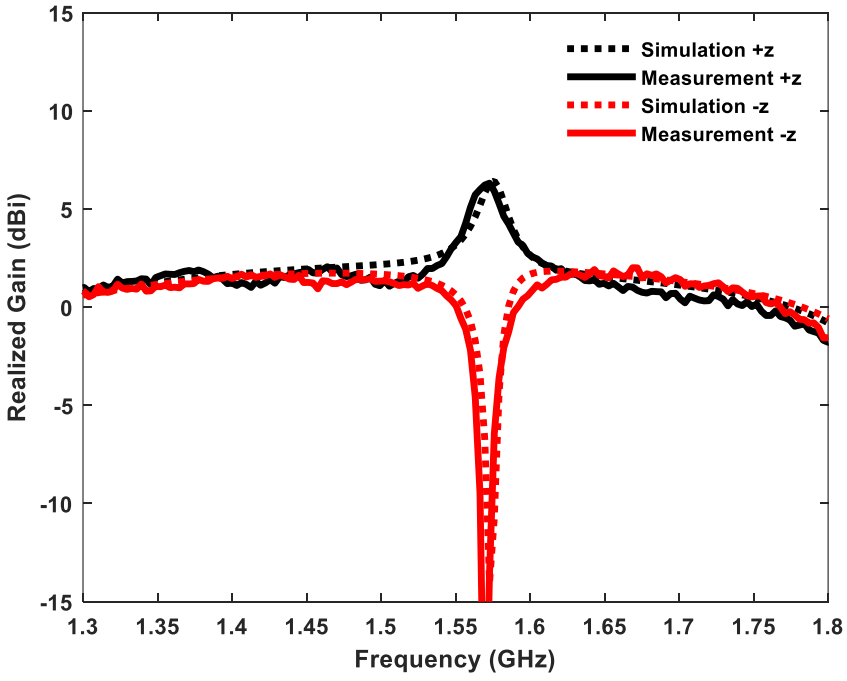

Fig. 3.9. Simulated and measured realized gain in the +*z* and -*z* direction.

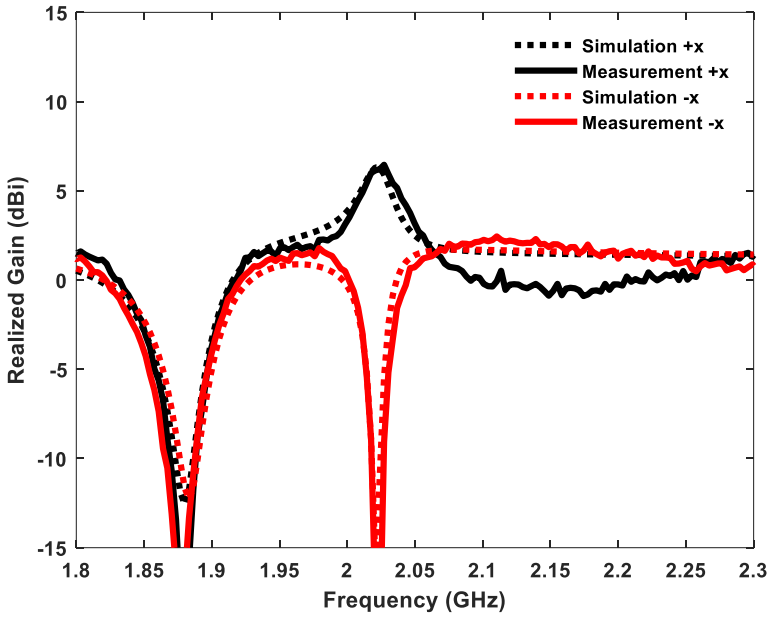

Fig. 3.10. Simulated and measured realized gain in the +*x* and -*x* direction.

The simulated and measured realized gain in the +*z* and -*z* direction versus frequency is shown in Fig. 3.9. The peak realized gain is observed to be 6.3 dBi at 1.573 GHz in the +*z* direction, with a front-to-back ratio of 19.8 dB. An excellent match to simulation in the lower band is observed. Next, the realized gain in the +*x* and -*x* direction is shown in Fig. 3.10. The peak realized gain in the +*x* direction is noted to be 6.2 dBi at 2.024 GHz, with a front-to-back ratio of 26.6 dB. There is a slight difference between simulation and measurement in the 2.1 GHz – 2.3 GHz range, with a slight front-to-back ratio observed. This is also likely due to the solder used during the fabrication process. Next, the simulated and measured impedance versus frequency is shown in Fig. 3.11. As expected, the high gain points shown above are active at an antiresonance. The simulated and measured normalized radiation patterns in the lower band are shown in Fig. 3.12. The patterns are taken at 1.480 GHz, 1.574 GHz, and 1.620 GHz. Fig. 3.12(a)(b)(c) are the patterns in the *xz* plane, and Fig. 3.12(d)(e)(f) are the patterns in the *yz* plane. A good match to simulation is observed in the lower band. Finally, the radiation patterns in the upper band are shown in Fig. 12. The patterns are taken at 1.956 GHz, 2.024 GHz, and 2.075 GHz. The *xz* plane is shown in Fig. 3.13(a)(b)(c), and the *yz* plane in Fig. 3.13(d)(e)(f). A good match to simulation is displayed.

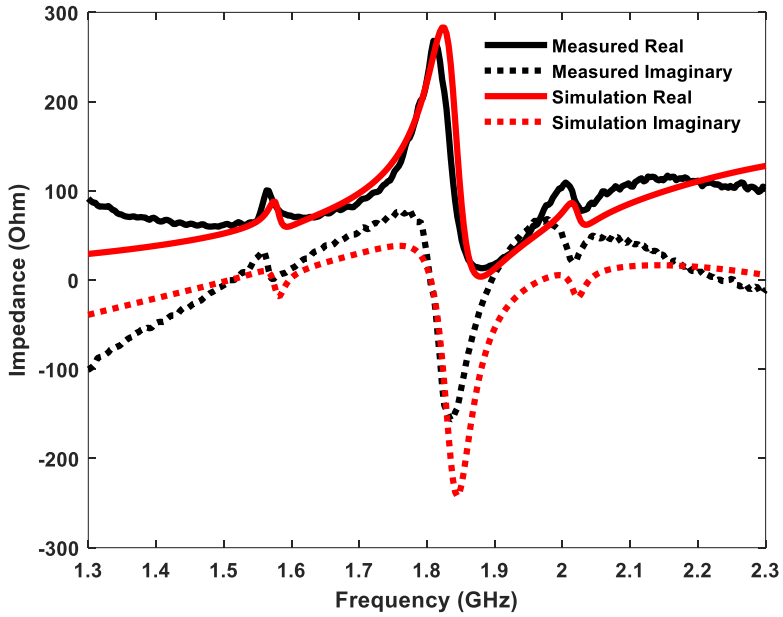

Fig. 3.11. Simulated and measured impedance versus frequency.

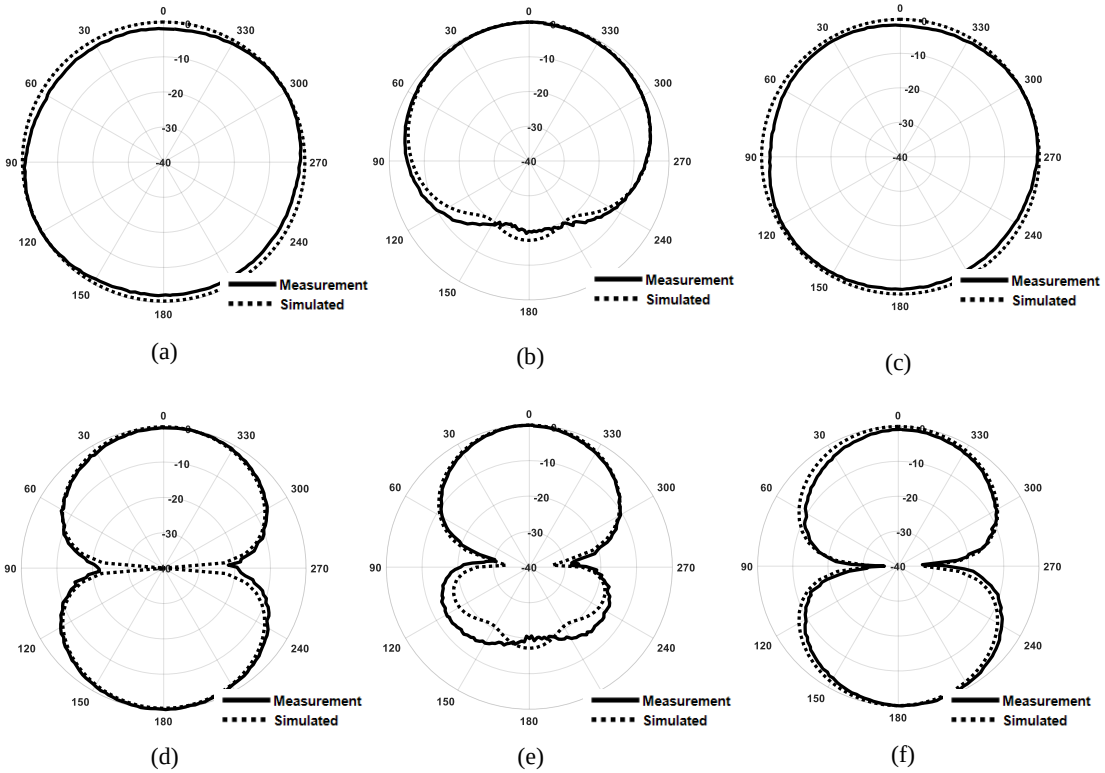

Fig. 3.12. Simulated and measured XZ and YZ normalized radiation patterns versus angle in the lower band. At (a) 1.48 GHz XZ, (b) 1.574 GHz XZ, (c) 1.620 GHz XZ, (d) 1.480 GHz YZ, (e) 1.574 GHz YZ, and (f) 1.620 GHz YZ.

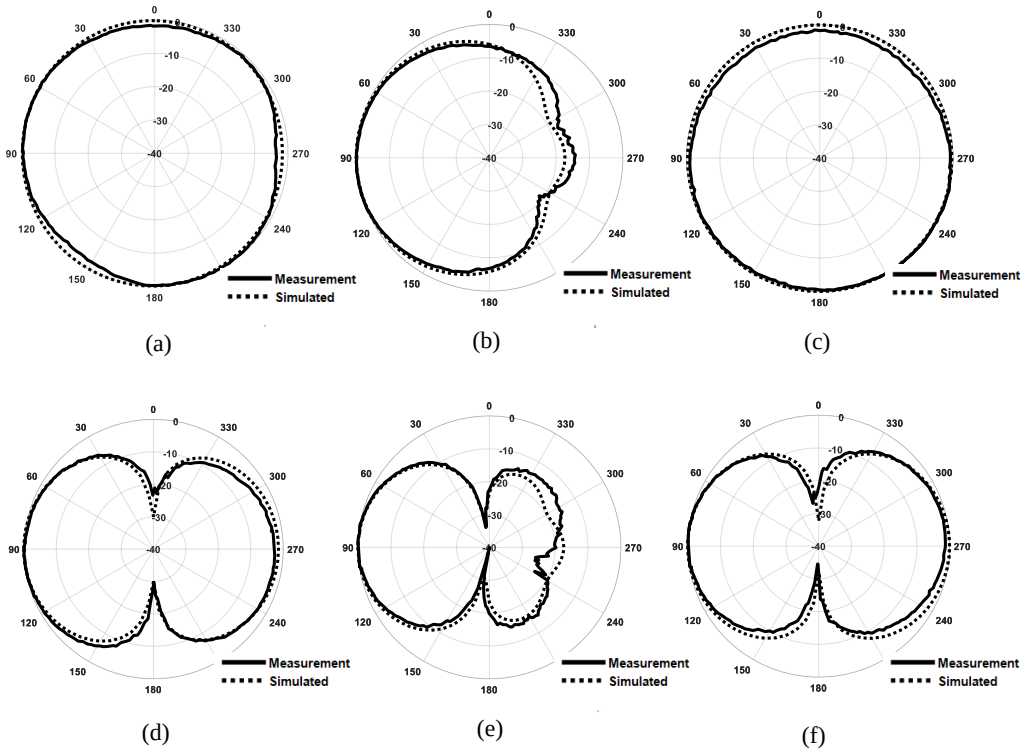

Fig. 3.13. Simulated and measured XZ and XY normalized radiation patterns versus angle in the upper band. At (a) 1.956 GHz XZ, (b) 2.024 GHz XZ, (c) 2.075 GHz XZ, (d) 1.956 GHz YZ, (e) 2.024 GHz YZ, and (f) 2.075 GHz YZ.

3.5 Conclusion

A quad-element, dual-band dipole with a high gain in both bands, as well as omni-directional modes in the azimuth plane is proposed in this chapter. Firstly, the design procedure for the quad-element dipole is shown. The antenna consists of a large dual element dipole to create the lower band, and a smaller dual-element dipole to create the upper band. These elements are combined at the feed, and the smaller element is rotated to be directive toward the +*x* direction, while the larger dual-element dipole is directive toward the +*z* direction. A prototype antenna is fabricated and measured to verify the results obtained in simulation. Solid agreement is found between the simulated and measured results. The measured antenna obtains a -10-dB IBW of 19.0% (1.268 GHz – 1.655 GHz) in the lower band, and 10.2% (1.960 GHz– 2.170 GHz) in the upper band. A peak realized gain in the +*z* direction of 6.3 dBi at 1.573 GHz, with a front-to-back ratio

of 19.8 dB, and a peak realized gain in the $+x$ direction of 6.2 dBi at 2.024 GHz, with a front-to-back ratio of 26.6 dB. The radiation patterns match the expected “Dipole mode” and high gain modes expected.

CHAPTER 4

A MULTIPLE-MODE DUAL-ELEMENT CROSS DIPOLE

4.1 Abstract

A single fed, broadband, dual-element crossed dipole is presented in this chapter. The dual-element cross dipole is optimized for realized gain and axial ratio with a GA, and the optimized length values are determined via an optimization study. The proposed antenna is simulated and measured for verification of the results obtained. The measured -10-dB IBW is 47.9% (1.37 GHz – 2.23 GHz). The 3-dB ARBW is 10.1% (1.707 GHz – 1.889 GHz), with an axial ratio minimum of 0.86 dB. Two points of peak gain are created at the combination points of the two dual-element dipoles. Their peak realized gain values are shown to be 6.03 dBi at 1.51 GHz, and 5.64 dBi at 2.1 GHz.

4.2 Introduction

The cross-dipole has been heavily used over many years due to its simple design and ability to generate circular polarization (CP) [37]. CP is created when two electric fields generate an equal magnitude and 90° phase difference signal. CP is created in the cross-dipole via a single feed and providing a length difference in the orthogonally connected dipole arms. This length difference generates CP. Extensive research has been performed on cross dipoles [38-46], and [7]. A cross-dipole antenna is used as a log-periodic dipole array (LPDA) element to generate CP [38]. Parasitic elements are added to the cross dipole to generate a high gain in [39], [7]. Broadband cross dipoles are reported in [40-45].

Broadband antennas are useful for a wide range of applications that can require a large frequency spectrum. An antenna that achieves broadband capability allows for space to be saved, as instead of using multiple antennas for different frequency bands the same antenna can be used. A broadband cross dipole is used with parasitic elements and bowtie dipole to achieve wideband capabilities [40]. An unequal power dividing network is used to create a broadband antenna [41-42]. A loop encircling the crossed dipole improves the bandwidth and performance of the antenna [43]. Dual-dipole antennas are shown to improve

the bandwidth of antennas [44-46]. A dual-dipole configuration is shown to nearly double the impedance bandwidth of a standard dipole antenna [2].

In combination with another element, a secondary, auxiliary element attached to the feed improves the impedance bandwidth performance. When these two elements are given a spacing value of 0.09λ a high realized gain value (6.3 dBi) is also noticed at the combination point of the two dipoles. This method of enhancing the bandwidth and gain of the antenna can be applied to a standard cross-dipole antenna.

In this chapter, a broadband dual-element cross-dipole antenna is proposed. Through the use of two cross dipoles connected at the feed, a broadband impedance bandwidth is observed. The proposed antenna is optimized using a genetic algorithm (GA) to achieve the highest realized gain and lowest axial ratio possible. A study is performed with the GA to find the best design frequency. The proposed antenna is then simulated using FEKO, and measured in an anechoic chamber using an Agilent Technologies E5063A vector network analyzer. Measurement is performed for verification of results found in simulation.

4.3 Antenna Design Procedure

A standard halfwave dipole is studied first in Fig. 1(a). A secondary, auxiliary dipole is then connected to the feed at a spacing of 0.09λ. The connection of the two dipoles is shown in Fig. 1(b). The larger dipole is placed on top in the $+z$ direction [2]. The corresponding reflection coefficient versus frequency is shown in Fig. 2, denoted by "Larger Dual-Dipole". A combination point where the two separate dipoles -10-dB IBW cross together under -10-dB.

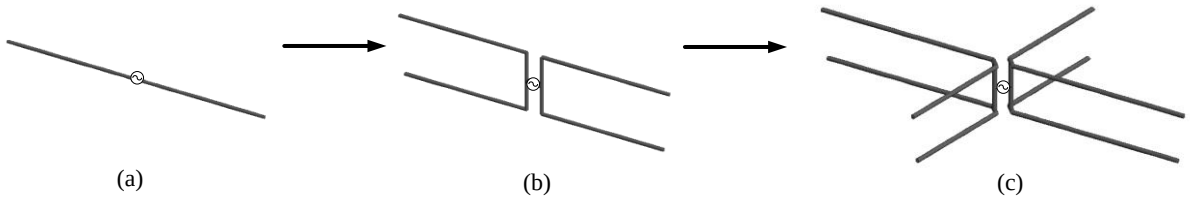

Fig. 4.1. Detailed design procedure of a quad-element dipole. (a) Standard halfwave dipole, (b) two dual element dipoles, and (c) proposed antenna.

Next, a second dual-element dipole is designed at a higher frequency, with a combination point at 2.13 GHz. This secondary dual-dipole is then attached to the feed after being rotated by φ = 90°. This setup mimics a crossed dipole. The feed spacing is set to 11 mm (.066λ), where λ is at 1.81 GHz. This combined antenna design is shown in Fig. 4.1(c). The reflection coefficient versus frequency is shown in Fig. 4.2. The corresponding combination points are slightly shifted down in frequency, this is due to the extra length added when combining the feeds. The corresponding impedance versus frequency plot is seen in Fig. 4.3. The plot shows the dual-element cross dipole in comparison to the two dual-element dipoles that make it up.

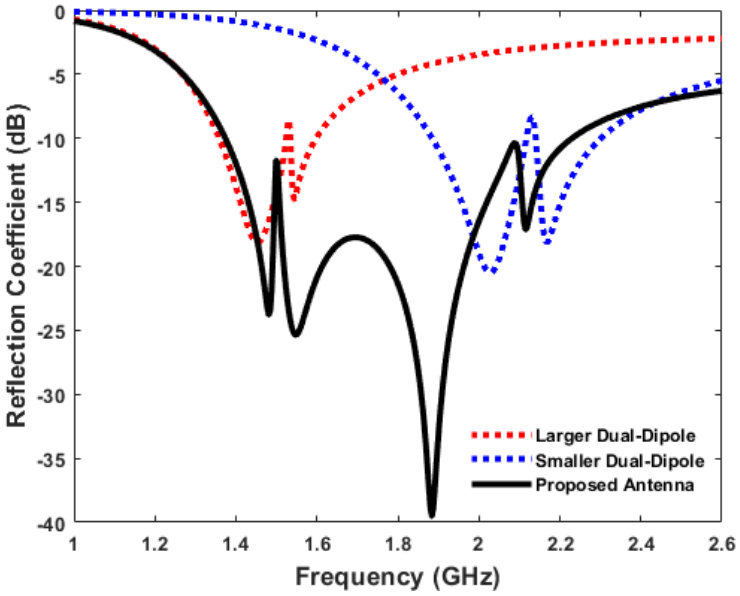

Fig. 4.2. Reflection coefficient versus frequency of Fig. 4.1(b)(c).

The two combination points both operate at antiresonances, causing the small bandwidth of the combination point, as shown in the previous plot the frequency is also slightly shifted down. When the antennas are combined an axial ratio dip is noticed at the center frequency of the total bandwidth. (1.81 GHz) Points of high gain similar to previous dual-dipole studies are also seen at the combination points.

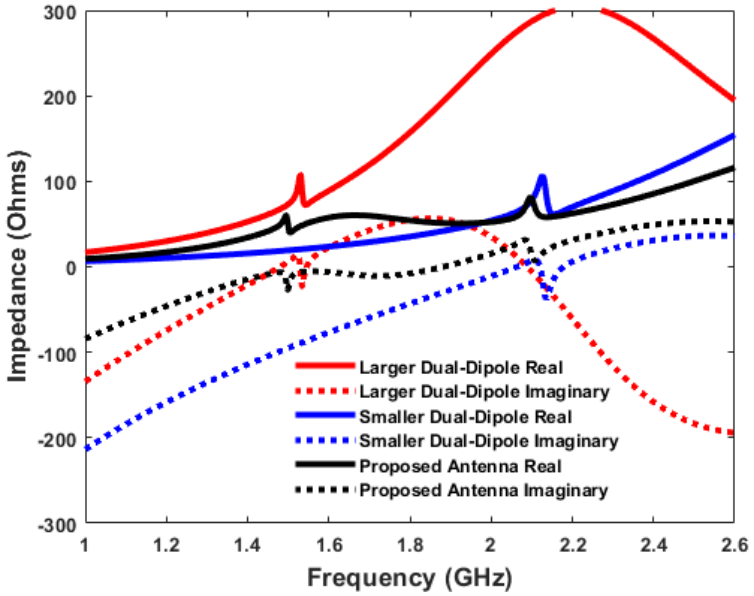

Fig. 4.3. Impedance versus frequency of (a) Fig. 4.1(b), and (b) Fig. 4.1(c).

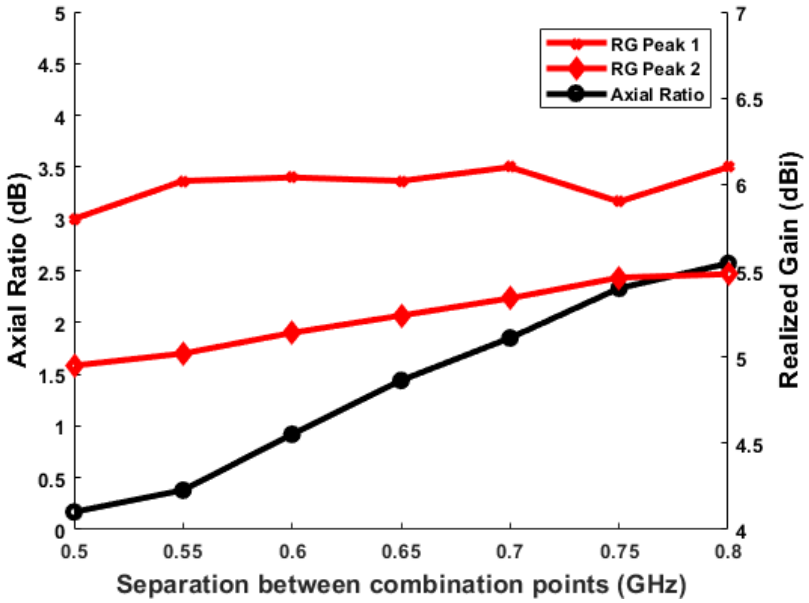

Fig. 4.4. Optimization results of Fig. 4.1(c).

Next, the antenna is optimized with a GA to improve the peak realized gain at both combination points, as well as decrease the axial ratio value at the center frequency. The cost function for the GA is as follows,

$$cost = wg_1(AR - 1) + wg_2(6 - RG)$$

Equation 4. Cost function for dual-element cross dipole.

AR is the axial ratio in the $+z$ direction, RG is the realized gain in the +z direction, and wg_1 and wg_2 are the weights. The weights are set at the following, $wg1 = 5$, and $wg2 = 1$. A higher weight is assigned to the axial ratio value as raising $wg2$ did not provide any noticeable increasement to the realized gain. An optimization study is performed in Fig. 4.4, between the difference in frequency of the two combination points, the realized gain, and the axial ratio at the center frequency (1.81 GHz). The plot starts at 1.50 GHz, and 2.00 GHz (0.5 GHz separation), and continues to 1.50 GHz, and 2.30 GHz (0.8 GHz separation). 8 different GA optimizations were performed. As the length difference increases, the RG at the second combination point also increases, however axial ratio also increases with the length difference.

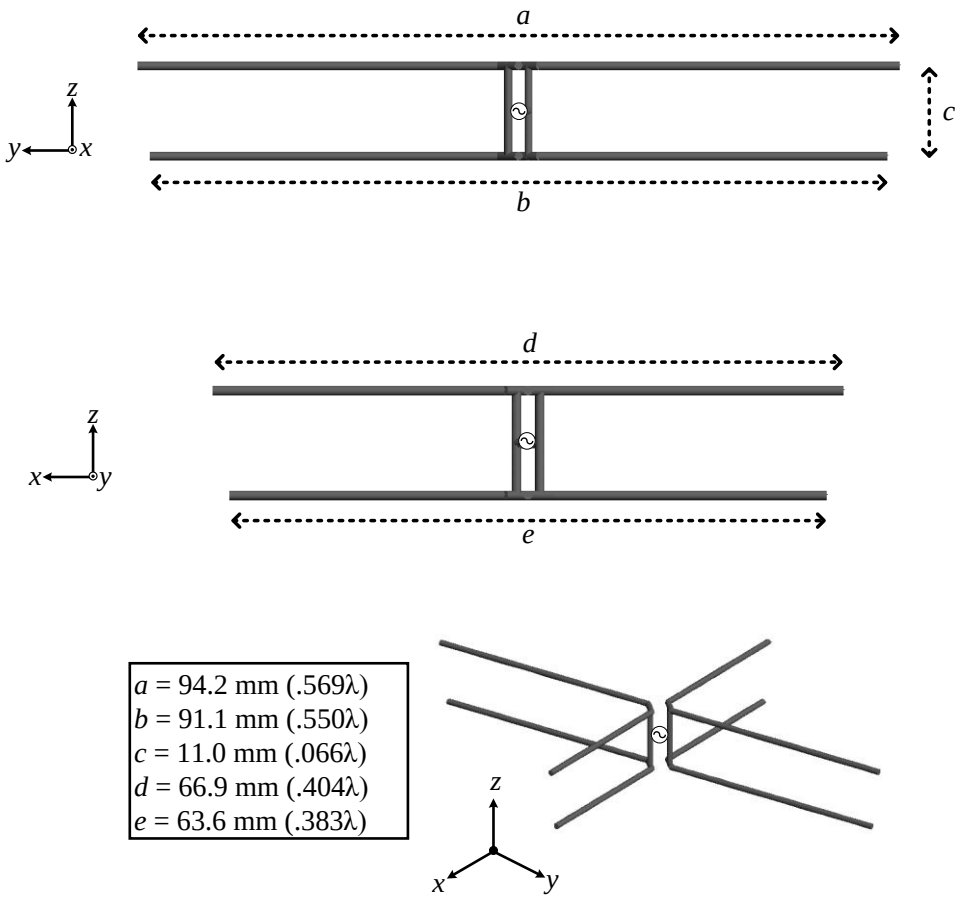

Fig. 4.5. Detailed geometry of the proposed antenna.

For example, at 0.5 GHz difference, the axial ratio is nearly 0 dB, however, the realized gain at the first point is barely above 5 dBi, while the RG at the second point is 5.9 dBi. The chosen separation value is 0.6 GHz, at this point the axial ratio is still below 1dB (0.92 dB), and the realized gain at both points is satisfactory (RG peak 1 = 6.0 dBi, RG peak 2 = 5.15 dBi).

After the values from the optimization study are chosen, the proposed antenna is simulated in Altair FEKO. The geometry of the proposed antenna is shown in Fig. 4.5. As noted in the original design procedure, the larger dipole is placed on top of the smaller dipole in the +*z* direction. The optimized lengths are a = 94.2 mm (0.569λ), b = 91.1 mm (0.550λ), c = 11.0 mm (0.066λ), d = 66.9 mm (0.404λ), and e = 63.6 mm (0.383λ). The proposed antenna demonstrates broadband capability with a continuous -10-dB IBW of 47.5% (1.37 GHz – 2.24 GHz). The axial ratio bandwidth (ARBW) is 10.5% (1.71 GHz – 1.90 GHz), with the AR minimum value occurring at 1.80 GHz (0.92 dB). Two RG peaks are observed within the bandwidth at the combination points shown in Fig. 2.

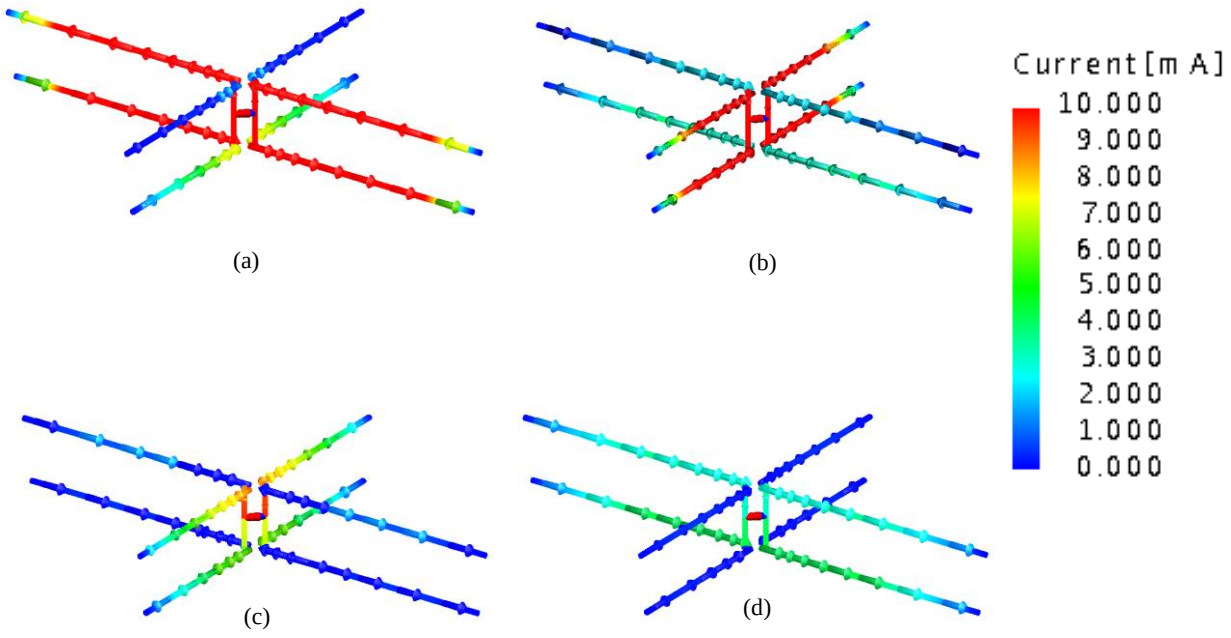

Fig. 4.6. Current analysis of a quad-element dipole. (a) 1.50 GHz 90° phase, (b) 2.10 GHz 140° phase, (c) 1.8 GHz 330° phase, and (d) 1.8 GHz 240° phase.

A current analysis is performed in Fig. 4.6 on the proposed antenna to examine the reasoning behind the two peak realized gain points (1.50 GHz, and 2.10 GHz), as well as the axial ratio generation (1.80 GHz). The current phase shown is the phase with the highest magnitude of current total. The value with a strong AR is shown at the peak magnitude, as well as a 90° phase difference from that point. Shown first in Fig. 4.6(a) is the first high realized gain mode at the combination point of the first dual dipole. Extremely strong currents are seen moving in opposite directions on the larger dual dipole in the *y* axis, similar to a Yagi antenna. Next, the second peak realized gain point is analyzed at 2.10 GHz, shown in Fig. 4.6(b). Extremely strong currents are seen on the dual dipole located on the *x* axis. Similar to Fig. 4.6(a), the currents are moving in opposite directions, this is also generating the point of high gain at the combination point of the dipoles. Finally, the axial ratio minimum point is analyzed at 1.8 GHz. The currents at this point are shown in Fig. 4.6(c)(d), the phase in Fig. 4.6(c) is 330°, while the phase in Fig. 4.6(d) is 240°. At 330° phase strong currents are seen in the dual dipole located on the *x* axis, while at 240° phase, strong currents are seen on the dipole located in the *y* axis. This axial ratio minimum is being generated as a combination of both dipoles in the *x* and *y* axis respectfully.

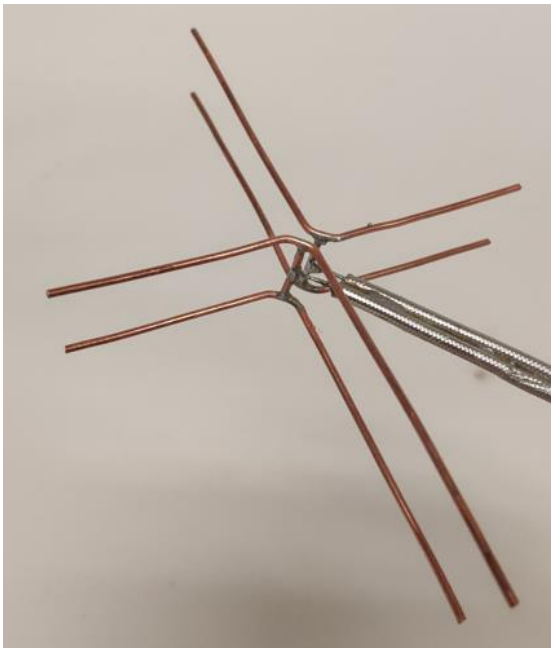

Fig. 4.7. Proposed Antenna.

4.4 Measurement Verification

A prototype of the dual-element cross dipole antenna is fabricated for verification of the results found in simulation. This prototype antenna is shown in Fig. 4.7. The wire radius used is AWG 18 (0.5 mm radius). The antenna is measured using an Agilent Technologies 5063A vector network analyzer. A Krytar model 4010265 180-degree hybrid balun is used to connect the antenna to the vector network analyzer. Two SMA coaxial cables are connected to the -3 dB output ports, and a 50-Ω load is applied to the sum port to ensure equal power distribution to the antenna.

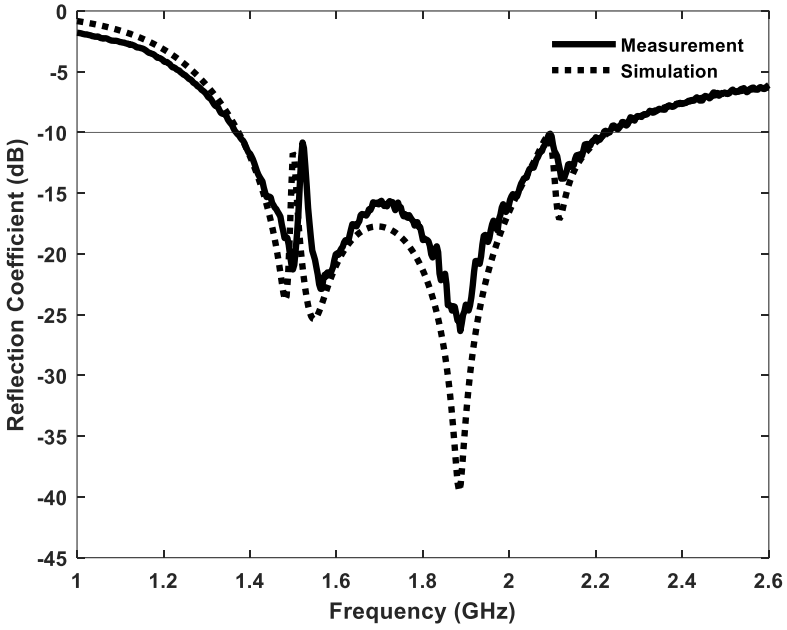

Fig. 4.8. Simulated and measured reflection coefficient versus frequency.

The simulated and measured reflection coefficient versus frequency is shown in Fig. 4.8. The measured -10-dB IBW of the antenna is 47.9% (1.57 GHz – 2.23 GHZ). This plot displays an excellent match to simulated values. Shown next is the simulated versus measured impedance versus frequency plot in Fig. 4.9. As expected, two antiresonances where the combination points occur at are observed. The first combination point is shown to have a slight shift in frequency, this matches to the reflection coefficient plot, where the combination point is also slightly shifted (1.50 GHz to 1.51 GHz).

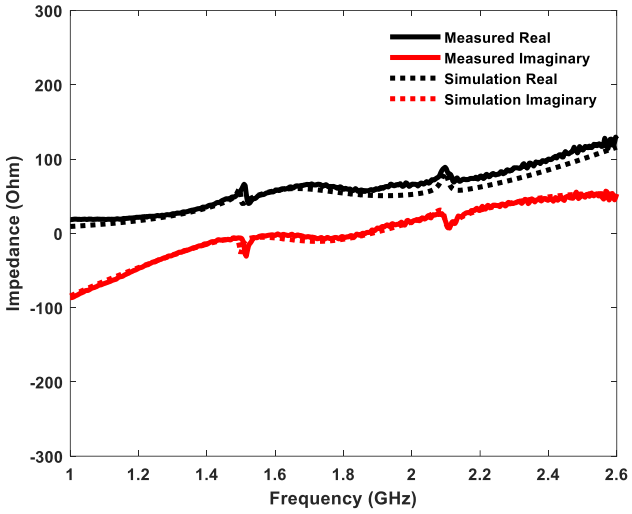

Fig. 4.9. Simulated and measured impedance versus frequency.

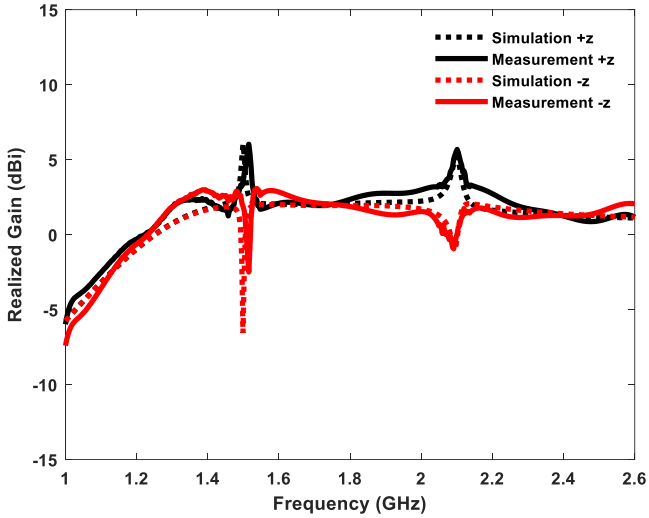

Fig. 4.10. Simulated and measured realized gain in the +*z* and -*z* direction.

Next, the simulated and measured realized gain versus frequency in the +*z* and -*z* direction is shown in Fig. 4.10. Two high realized gain points are observed, both at the antiresonances shown in Fig. 4.9. The first point is at 1.51 GHz, and displays a peak realized gain of 6.03 dBi. The second point is at 2.10 GHz, and displays a peak realized gain of 5.64 dBi. The frequency shift of the first realized gain point is consistent with both the reflection coefficient, and the impedance plots. A slight shift in the frequency is likely caused by solder used during the fabrication process.

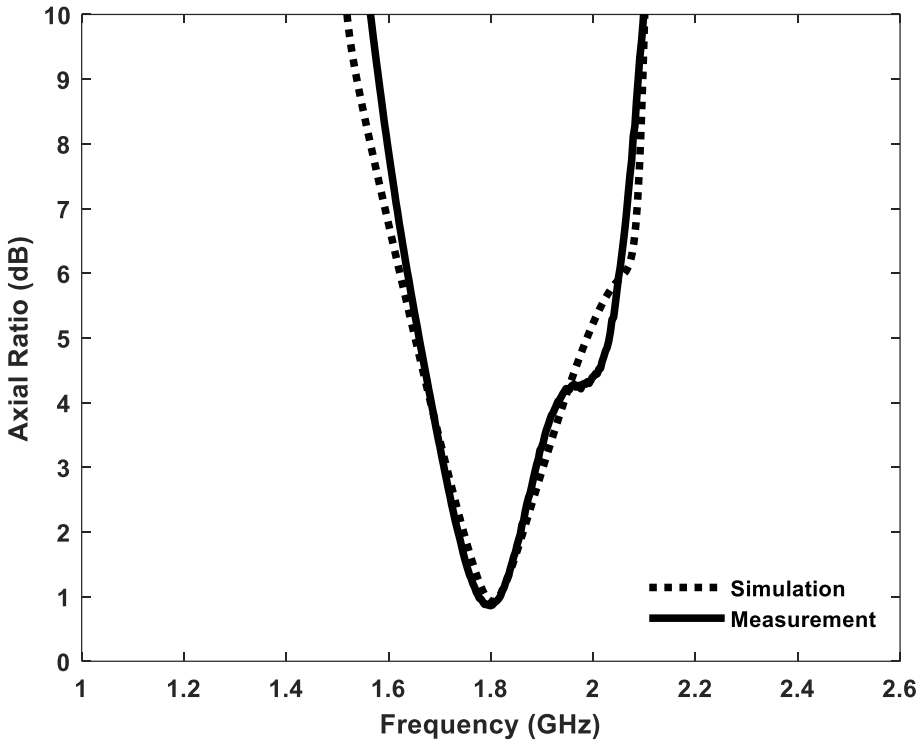

Fig. 4.11. Simulated and measured axial ratio in the +z versus frequency.

Next, the simulated and measured axial ratio versus frequency in the +z direction is displayed in Fig. 4.11. The 3-dB axial ratio bandwidth is 10.1% (1.707 GHz – 1.889 GHz). An axial ratio minimum of 0.86 dB is observed at 1.80 GHz.

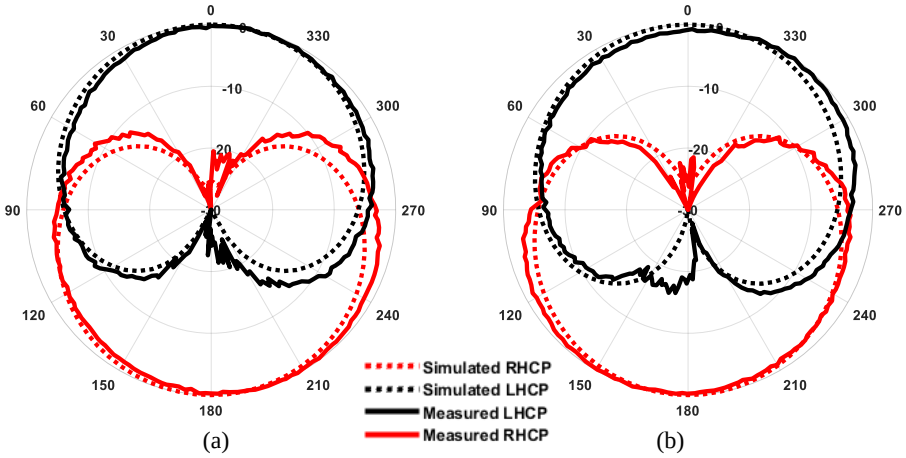

Fig. 4.12. Simulated and measured (a) XZ and (b) YZ normalized LHCP and RHCP patterns at 1.8 GHz.

This axial ratio demonstrates that the antenna is perfectly CP at 1.8 GHz. The normalized right hand circular polarization (RHCP) and the left hand circular polarization (LHCP) plots at this point (1.80 GHz) in the *xz* and *yz* planes are shown in Fig. 4.12. The antenna displays a strong LHCP component in the +*z* direction, and a strong RHCP component in the -*z* direction. It is observed that in the +*z* direction there is a difference of over 15 dB between RHCP and LHCP components, this indicates that the antenna is strongly CP at this point.

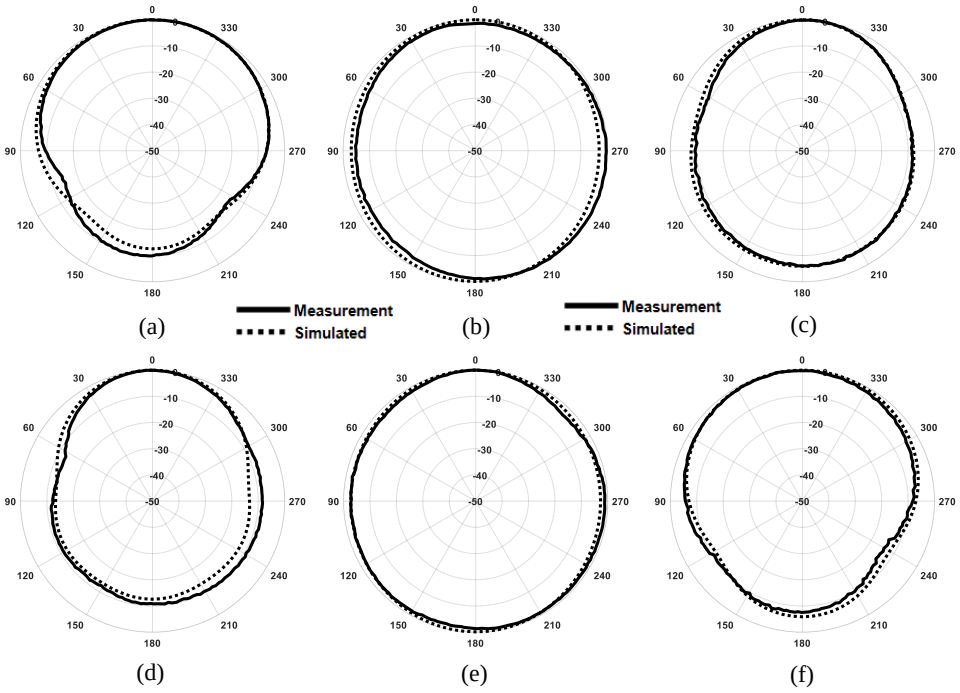

Fig. 4.13. Simulated and measured XZ and YZ normalized radiation patterns versus angle. At (a) 1.50 GHz XZ, (b) 1.80 GHz XZ, (c) 2.10 GHz XZ, (d) 1.5 GHz YZ, (e) 1.80 GHz YZ, and (f) 2.10 GHz YZ.

Finally, the normalized radiation patterns versus angle in the *xz* and *yz* planes are shown in Fig. 4.13. The frequencies chosen are 1.50 GHz (high gain mode), 1.80 GHz (CP mode), and 2.10 GHz (high gain mode). The patterns at all frequencies provide a good match to simulated values. It is also consistent with the current analysis in Fig. 4.6, where the high gain modes are observed at the point where strong opposite currents are present on their respective dual-element dipoles.

4.5 Conclusion

A multiple mode, dual-element cross dipole is presented in this chapter. Firstly, an optimization study is performed on a dual-element cross dipole antenna, it is found that the separation for the peaks is most optimal at 0.6 GHz. This separation displays a good axial ratio, without sacrificing too much forward realized gain. Next, a current analysis is performed to determine the cause of the high gain points seen at the combination point of the two dual-element dipoles, as well as determine where circular polarization is being created. A prototype antenna is fabricated and measured to verify the results found within simulation. Great agreement between simulation and measurement is observed. The measured antenna displays a -10-dB IBW of 47.9% (1.37 GHz – 2.23 GHz). A 3-dB axial ratio bandwidth of 10.1% (1.707 GHz – 1.889 GHz), with a minimum value of 0.86 dB. The multiple mode function is also verified, three distinct “dipole modes” are observed at 1.4 GHz, 1.8 GHz, and 2.2 GHz, with a CP mode at 1.8 GHz. Two high gain modes are observed at 1.51 GHz, and 2.10 GHz, with a peak value of 6.03 dBi, and 5.64 dBi respectfully.

CHAPTER 5

CONCLUSION

5.1 Conclusion

In this thesis, dual-element dipole applications are investigated. These applications all show similar traits of the dual-element dipole, with a dipole like mode, and a high gain mode within each bandwidth being a common factor. The bandwidth of each original element is also consistently enhanced. Firstly, in chapter 1, a background is given on specific topics that pertain to the work performed in this thesis. The background is given on dual-element dipoles, Yagi antennas, dual-band antennas, circular polarization, and how measurements in this thesis are performed.

Next, in chapter 2, a dual-element dipole design is proposed with a high gain and minimal front-to-back ratio outside of Yagi mode. An investigation is performed on this antenna to find the reasoning behind the creation of the high gain mode at the combination point of the dipoles. It is found that the equal magnitude and opposite current directions generate this high gain point, similar to a Yagi antenna. This antenna nearly doubles the normal -10-dB IBW of a standard dipole (10% to 19.3%), as well as offering a high gain mode within the bandwidth.

Next, in chapter 3, a quad-element dipole with dual-band capabilities is proposed. This design takes two dual-element dipoles designed at different resonant frequencies and connects them together at the feed. The antenna demonstrates dual-band capability with two resonant frequencies. In both of these bandwidths two dipole modes, and a high gain mode are observed. The lower band element is directive toward the $+z$ direction, and the upper band element is directive toward the $+x$ direction.

Finally, in chapter 4, a broadband, multiple mode, dual-element cross-dipole antenna is proposed and analyzed. A comprehensive design procedure with the help of a GA is shown. The optimized design is taken from an optimization study with realized gain, and axial ratio as the parameters. The antenna demonstrates broadband capability, with two high gain points at both of the combination points of the two dual-dipoles. CP generation is also achieved at the center frequency of the bandwidth. With this there are 3 separate modes achieved in this antenna, dipole mode, high gain mode, and CP mode.

REFERENCES

[1] K. D. Xu, D. Li, Y. Liu and Q. H. Liu, "Printed Quasi-Yagi Antennas Using Double Dipoles and Stub-Loaded Technique for Multi-Band and Broadband Applications," *IEEE Access*, vol. 6, pp. 31695-31702, 2018.

[2] G. Evans and S. Lim, "Spacing Analysis of a Dual-Element Dipole," *Proc. Int. Symp. Antennas Propag*., Denver, CO, USA, 2022.

[3] H. Yagi, and S. Uda. "Projector of the sharpest beam of electric waves." *Proc. Of the imperial Academ. of Japan*, 1926: 49-52

[4] L. P. Smith, J. C. Howell and S. Lim, "A Size-Reduced, 15-Element, Planar Yagi Antenna *IEEE Trans. Antennas Propag*., vol. 69, no. 4, pp. 2410-2415, April 2021.

[5] A. T. Mobashsher, M. T. Islam and N. Misran, "A Novel High-Gain Dual-Band Antenna for RFID Reader Applications," *IEEE Antennas Wireless Propag. Lett.*, vol. 9, pp. 653-656, 2010.

[6] B. Y. Toh, R. Cahill and V. F. Fusco, "Understanding and measuring circular polarization," *IEEE Trans. Edu.*, vol. 46, no. 3, pp. 313-318, Aug. 2003.

[7] S. Lim, J. Chen and C. Cato, "Design of a Thin, Electrically Small, Two-Element Parasitic Array With Circular Polarization," *IEEE Antennas Wireless Propag. Lett.,*, vol. 17, no. 6, pp. 1006-1009, June 2018.

[8] S. Lim and H. Ling, "Design of a closely spaced, folded Yagi antenna," *IEEE Antennas Wireless Propag. Lett.*, vol. 5, pp. 302–305, 2006.

[9] Q. Xin, F.-S. Zhang, B.-H. Sun, Y.-L. Zou, and Q.-Z. Liu, "Yagi-Uda antenna with small size for vehicles," *Electron. Lett.*, vol. 47, no. 7, pp. 428–430, 2011.

[10] D. Arceo and C. A. Balanis, "A compact Yagi–Uda antenna with enhanced bandwidth," *IEEE Antennas Wireless Propag. Lett.*, vol. 10, pp. 442–445, 2011.

[11] Z. Bayraktar, P. L. Werner, and D. H. Werner, "The design of miniature three-element stochastic Yagi-Uda arrays using particle swarm optimization," *IEEE Antennas Wireless Propag. Lett*., vol. 5, pp. 22–26, 2006.

[12] J. J. Yu and S. Lim, "Design of multi-band, compact parasitic array with twisted, helical directors," *IEEE Trans. Antennas Propag.*, vol. 61, no. 1, pp. 444–449, Jan. 2013.

[13] J. Yu, Y. Le, and S. Lim, "Design of a dual-band, electrically small, parasitic array antenna," *IEEE Antennas Wireless Propag. Lett.*, vol. 13, pp. 1453–1456, 2014.

[14] Z. Hu, Z. Shen, W. Wu, and J. Lu, "Low-profile top-hat monopole Yagi antenna for end-fire radiation," *IEEE Trans. Antennas Propag*., vol. 63, no. 7, pp. 2851–2857, Jul. 2015.

[15] S. Lim and M. F. Iskander, "Design of a Dual-Band, Compact Yagi Antenna Over an EBG Ground Plane," *IEEE Antennas Wireless Propag. Lett.*, vol. 8, pp. 88-91, 2009.

[16] Y. Luo and Q. -X. Chu, "A Yagi–Uda Antenna With a Stepped-Width Reflector Shorter Than the Driven Element," *IEEE Antennas Wireless Propag. Lett.*, vol. 15, pp. 564-567, 2016.

[17] J. Yeo and J. -I. Lee, "Bandwidth Enhancement of Double-Dipole Quasi-Yagi Antenna Using Stepped Slotline Structure," *IEEE Antennas Wireless Propag. Lett.*, vol. 15, pp. 694-697, 2016.

[18] K. Anim and Y. -B. Jung, "Shortened Log-Periodic Dipole Antenna Using Printed Dual-Band Dipole Elements," *IEEE Trans. Antennas Propag*., vol. 66, no. 12, pp. 6762-6771, Dec. 2018.

[19] Y. Quan, H. Wang, S. Tao and J. Yang, "A Wideband Endfire Double Dipole Antenna Fed From Double-Ridge Gap Waveguides for Multibeam Array Application," *IEEE Antennas Wireless Propag. Lett.*, vol. 21, no. 4, pp. 760-764, April 2022.

[20] N. Patwari and A. Safaai-Jazi, "High-gain low-sidelobe double-vee dipoles *IEEE Trans. Antennas Propag*., vol. 48, no. 2, pp. 333-335, Feb. 2000.

[21] E. E. Altshuler, T. H. O'Donnell, A. D. Yaghjian and S. R. Best, "A monopole superdirective array," *IEEE Trans. Antennas Propag*., vol. 53, no. 8, pp. 2653-2661, Aug. 2005.

[22] W. Liang, Y. -C. Jiao, Y. Luan and C. Tian, "A Dual-Band Circularly Polarized Complementary Antenna" *IEEE Antennas Wireless Propag. Lett.*, vol. 14, pp. 1153-1156, 2015.

[23] W. C. Mok, S. H. Wong, K. M. Luk and K. F. Lee, "Single-Layer Single-Patch Dual-Band and Triple-Band Patch Antennas," *IEEE Trans. Antennas Propag*., vol. 61, no. 8, pp. 4341-4344, Aug. 2013.

[24] J. Anguera, E. Martinez-Ortigosa, C. Puente, C. Borja and J. Soler, "Broadband Triple-Frequency Microstrip Patch Radiator Combining a Dual-Band Modified Sierpinski Fractal and a Monoband Antenna," *IEEE Trans. Antennas Propag*., vol. 54, no. 11.

[25] S. K. Mishra, R. K. Gupta, A. Vaidya and J. Mukherjee, "A Compact Dual-Band Fork-Shaped Monopole Antenna for Bluetooth and UWB Applications," *IEEE Antennas Wireless Propag. Lett.*, vol. 10, pp. 627-630, 2011.

[26] J. Malik, A. Patnaik and M. V. Kartikeyan, "A Compact Dual-Band Antenna With Omnidirectional Radiation Pattern," *IEEE Antennas Wireless Propag. Lett.*, vol. 14, pp. 503-506, 2015.

[27] Y. Gu, X. -X. Yang, T. Lou and Y. Wu, "Low-Profile Dual-Band Magneto-Electric Dipole Antenna Loaded With Metasurface," *IEEE Antennas Wireless Propag. Lett.*, vol. 21, no. 7, pp. 1492-1496, July 2022.

[28] K. He, S. -X. Gong and F. Gao, "A Wideband Dual-Band Magneto-Electric Dipole Antenna With Improved Feeding Structure," *IEEE Antennas Wireless Propag. Lett.*, vol. 13, pp. 1729-1732, 2014.

[29] C. -Y. Shuai and G. -M. Wang, "A Novel Planar Printed Dual-Band Magneto-Electric Dipole Antenna," *IEEE Access*, vol. 5, pp. 10062-10067, 2017.

[30] K. Niotaki, S. Kim, S. Jeong, A. Collado, A. Georgiadis and M. M. Tentzeris, "A Compact Dual-Band Rectenna Using Slot-Loaded Dual Band Folded Dipole Antenna," *IEEE Antennas Wireless Propag. Lett.*, vol. 12, pp. 1634-1637, 2013.

[31] Z. Wang, G. -x. Zhang, Y. Yin and J. Wu, "Design of a Dual-Band High-Gain Antenna Array for WLAN and WiMAX Base Station," *IEEE Antennas Wireless Propag. Lett.*, vol. 13, pp. 1721-1724, 2014.

[32] I. T. Nassar, H. Tsang, D. Bardroff, C. P. Lusk and T. M. Weller, "Mechanically Reconfigurable, Dual-Band Slot Dipole Antennas," *IEEE Trans. Antennas Propag*., vol. 63, no. 7, pp. 3267-3271, July 2015.

[33] H. Zhang and H. Xin, "A Dual-Band Dipole Antenna With Integrated-Balun," *IEEE Trans. Antennas Propag*., vol. 57, no. 3, pp. 786-789, March 2009.

[34] S. A. Alekseytsev and A. P. Gorbachev, "The Novel Printed Dual-Band Quasi-Yagi Antenna With End-Fed Dipole-Like Driver," *IEEE Trans. Antennas Propag*., vol. 68, no. 5, pp. 4088-4090, May 2020.

[35] Jhin-Fang Huang, Mao-Hsiu Hsu and Jia-Wei Liang, "Wideband printed and double-sided dipole pair antennas with a parallel reflector," *2005 IEEE Internat. Symp. Micro*., Antenna, Propagation and EMC Technologies for Wireless Communications, Beijing, China, 2005.

[36] J. -f. Huang, M. -h. Hsu and F. -j. Wu, "Design of a Double-Sided and Printed Wideband Dipole Array Antenna on 5.2GHz Band," 2006 6th Internat. *Conf. ITS Telecomm.*, Chengdu, China, 2006.

[37] M. F. Bolster, "A New Type of Circular Polarizer Using Crossed Dipoles," *IRE Trans. Micro. Theory Tech.*, vol. 9, no. 5, pp. 385-388, September 1961.

[38] K. A. Leon, J. Haney and S. Lim, "A Size-Reduced, Circularly Polarized, Log-Periodic Dipole Array," *IEEE Antennas Wireless Propag. Lett.*, vol. 21, no. 2, pp. 371-375, Feb. 2022.

[39] L. Wang, W. -X. Fang, Y. -F. En, Y. Huang, W. -H. Shao and B. Yao, "Wideband Circularly Polarized Cross-Dipole Antenna With Parasitic Elements," *IEEE Access*, vol. 7, pp. 35097-35102, 2019.

[40] G. Feng, L. Chen, X. Wang, X. Xue and X. Shi, "Broadband Circularly Polarized Crossed Bowtie Dipole Antenna Loaded With Parasitic Elements," *IEEE Antennas Wireless Propag. Lett.*, vol. 17, no. 1, pp. 114-117, Jan. 2018.

[41] R. Xu, J. -Y. Li and W. Kun, "A Broadband Circularly Polarized Crossed-Dipole Antenna," *IEEE Trans. Antennas Propag*., vol. 64, no. 10, pp. 4509-4513, Oct. 2016.

[42] Y. He, W. He and H. Wong, "A Wideband Circularly Polarized Cross-Dipole Antenna," *IEEE Antennas Wireless Propag. Lett.*, vol. 13, pp. 67-70, 2014.

[43] G. Feng, L. Chen, X. Xue and X. Shi, "Broadband Circularly Polarized Crossed-Dipole Antenna With a Single Asymmetrical Cross-Loop," *IEEE Antennas Wireless Propag. Lett.*, vol. 16, pp. 3184-3187, 2017.

[44] S. X. Ta and I. Park, "Crossed Dipole Loaded With Magneto-Electric Dipole for Wideband and Wide-Beam Circularly Polarized Radiation," *IEEE Antennas Wireless Propag. Lett.*, vol. 14, pp. 358-361, 2015.

[45] L. Wang, W. -X. Fang, W. -H. Shao, B. Yao, Y. Huang and Y. -F. En, "Broadband Circularly Polarized Cross-Dipole Antenna With Multiple Modes," *IEEE Access*, vol. 8, pp. 66489-66494, 2020.

[46] F. -P. Lai, J. -F. Yang and Y. -S. Chen, "Compact Dual-Band Circularly Polarized Antenna Using Double Cross Dipoles for RFID Handheld Readers," *IEEE Antennas Wireless Propag. Lett.*, vol. 19, no. 8, pp. 1429-1433, Aug. 2020.